NOTICE

AVIS

The quality of this microform is heavily dependent upon the quality of the original thesis submitted for microfilming. Every effort has been made to ensure the highest quality of reproduction possible.

La qualité de cette microforme dépend grandement de la qualité de la thèse soumise au microfilmage. Nous avons tout fait pour assurer une qualité supérieure de reproduction.

If pages are missing, contact the university which granted the degree.

S'il manque des pages, veuillez communiquer avec l'université qui a conféré le grade.

Some pages may have indistinct print especially if the original pages were typed with a poor typewriter ribbon or if the university sent us an inferior photocopy.

La qualité d'impression de certaines pages peut laisser à désirer, surtout si les pages originales ont été dactylographiées à l'aide d'un ruban usé ou si l'université nous a fait parvenir une photocopie de qualité inférieure.

Reproduction in full or in part of this microform is governed by the Canadian Copyright Act, R.S.C. 1970, c. C-30, and subsequent amendments.

La reproduction, même partielle, de cette microforme est soumise à la Loi canadienne sur le droit d'auteur, SRC 1970, c. C-30, et ses amendements subséquents.

Canada

UNIVERSITY OF ALBERTA

The APPLICATION OF MICRO-MACHINING TECHNOLOGY FOR THE
CONSTRUCTION OF END-COLUMN CONDUCTIVITY DETECTOR IN
CAPILLARY ZONE ELECTROPHORESIS

BY

CHUNHONG PENG $\copyright$

A THESIS SUBMITTED TO THE FACULTY OF GRADUATE STUDIES AND
RESEARCH IN PARTIAL FULFILLMENT OF THE REQUIREMENTS FOR THE
DEGREE OF

MASTER OF SCIENCE

DEPARTMENT OF CHEMISTRY

EDMONTON, ALBERTA

SPRING, 1993

UNIVERSITY OF ALBERTA

RELEASE FORM

NAME OF AUTHOR :   CHUNHONG PENG

TITLE OF THESIS :   The Application Of Micro-Machining Technology For The

Construction Of End-Column Conductivity Detector In

Capillary Zone Electrophoresis

DEGREE :   MASTER OF SCIENCE

YEAR THIS DEGREE GRANTED : 1993

Permission is hereby granted to the University of Alberta Library to reproduce single copies of this thesis and to lend or sell such copies for private, scholarly or scientific research purposes only.

The author reserves all other publication and other rights in association with the copyright in the thesis, and except as hereinbefore provided neither the thesis nor any substantial portion thereof may be printed or otherwise reproduced in any material form whatever without the author' s prior written permission.

Feburary 16, 1993

UNIVERSITY OF ALBERTA
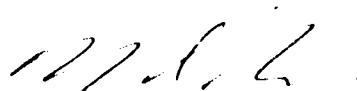
FACULTY OF GRADUATE STUDIES AND RESEARCH

The undersigned certify that they have read, and recommend to the Faculty of Graduate Studies and Research for acceptance, a thesis entitled
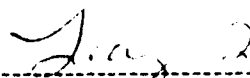
THE APPLICATION OF MICRO-MACHINING TECHNOLOGY FOR THE CONSTRUCTION OF END-COLUMN CONDUCTIVITY DETECTOR IN CAPILLARY ZONE ELECTROPHORESIS submitted by

CHUNHONG PENG
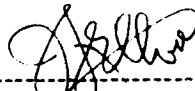
in partial fulfillment of the requirements for the degree of MASTER OF SCIENCE

Dr. Norman J. Dovichi (supervisor)

Dr. Liang Li

Dr. John Elliott

January 19, 1993

ABSTRACT

In this thesis, a micro-machining technique based on a wafer dicing saw was used to construct an end-column electrical conductivity detector in capillary zone electrophoresis. This micro machining technique was used to dice narrow slits on many fused-silica capillaries with the size accurately controlled. The technique presents high dicing efficiency, hundreds of slits can be made on 50 μm ~ 200 μm i.d. fused-silica capillaries within 20 minutes. Another important application of the wafer dicing saw is making holes indirectly with controllable size across the capillary. This is the simplest but state-of-the-art non-laser technique to make holes on the fused-silica capillaries. Under the TV monitor of the wafer dicing saw, a 55 μm wide x 110 μm deep slit was diced longitudinally on the centre of the internal hole of 75 μm i.d. fused-silica capillaries. The capillary was then aligned with another smooth cross-section capillary under a microscope. The two capillaries were melted together by a micro-torch under microscope at about 1300 °C. Amazingly, the slit was not distorted by 1300 °C high temperature.

For the construction of the end-column electrical conductivity detector, a 48 μm thick resin blade was selected to dice a 164 μm deep x 55 μm wide slit exactly 10 mm from the cathodic end of 52 μm i.d. x 360 μm o.d. fused-silica capillary. Under microscope, a 15 mm long x 50.8 μm diameter platinum wire was then inserted to the middle of the slit as sensing electrode. The capillary tip and 50.8 μm platinum wire were then sealed by Araldite epoxy adhesive under microscope. The other end of the 50.8 diameter platinum was soldered to a coaxial cable and sealed again. The detector was constructed on a 1/8" i.d. x 1/4" o.d. Plexiglas tubing. The conductivity signal was measured between the sensing electrode inside the capillary and the grounding electrode with a home-made electronic circuit. The end-column conductivity detector did not suffer from electrical interference caused by the applied high voltage during the electrophoresis.

Li^+, Na^+ and K^+ were used to calibrate the detector. The concentration detection limit based on Knoll's method (44) reaches 7.4×10^{-7} M, 4.8×10^{-7} M and 2.6×10^{-7} for Li^+, Na^+ and K^+. The maximum number of theoretical plates achieved was more than 150,000 for Li^+. The detection limit and separation efficiency are comparable to literature values (30,36,37). Li^+, Na^+, K^+ and Rb^+ were well separated within 4 minutes when 20 mM MES / histidine (pH = 6.15) was used as electrophoretic buffer at 250 V / cm electric field.

ACKNOWLEDGMENTS

TABLE OF CONTENTS

LIST OF FIGURES

LIST OF TABLES

CHAPTER I

INTRODUCTION TO OPEN TUBULAR
CAPILLARY ZONE ELECTROPHORESIS

1.1 Theory of capillary zone electrophoresis

Electrophoresis is the separation of charged species based on differential migration at an applied electric field. It was first described by Arne Tiselius in his Ph.D. thesis in 1930 and published in 1937 (76). In 1967, Hjerten presented the pioneering demonstration of capillary electrophoresis by using 3 mm i.d. diameter capillaries under high electric field (29). In 1974, Virtanen described the electrophoretic separation in 0.2 ~ 0.5 mm i.d. glass tubes by potentiometric detection (80). In 1979, Mikkers and Everaerts performed the separation of organic and inorganic anions in 0.2 mm i.d. Teflon capillary with either UV or conductivity detection (54,55). However, they were unable to achieve high separation efficiency because of sample overloading. In 1981, Jorgensen and Lukacs demonstrated the first high efficiency separation with more than 400,000 theoretical plates using narrow bore glass capillary (38). This work has become the landmark in capillary zone electrophoresis and been quoted for thousands of times.

1.1.1 Electrophoresis

In capillary zone electrophoresis, a narrow plug of sample is introduced into the buffer-filled capillary from the high voltage end as illustrated in figure 1.1. When high electric field is applied across the capillary, different species in the sample migrate differentially according to the individual ionic mobility. The mobility of an ion at any finite equivalent concentration is the velocity with which the ion moves under unit potential gradient (88). Its unit is m^2 / V sec equiv. At infinite dilution, the ionic mobility reaches a limiting maximum value called absolute mobility, μ^o. Ionic mobility is affected by the solute properties such as shape, Stokes' radius and charge. The ionic mobility of an aqueous solution rises about 2 % per °C (50,65). The interaction of the solutes with the carrier buffer may also influence the ionic mobility. Figure 1.2 is the cross-section of the fused-silica capillary with polyimide coating.

capillary

detector

+ high

voltage

buffer

μA

Plexiglas box
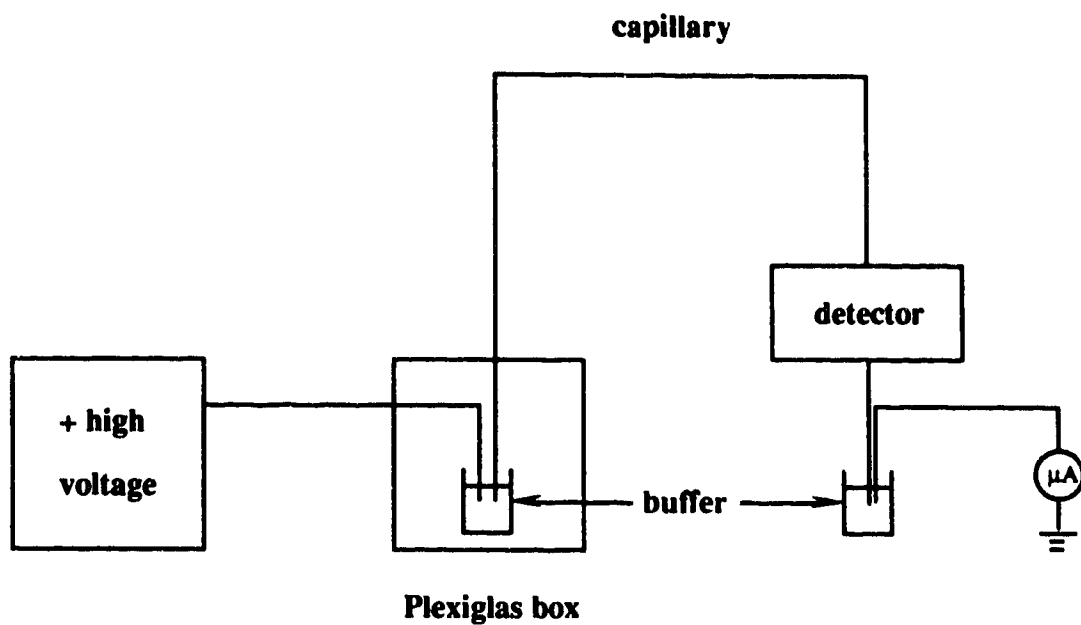
Figure 1.1

Instrumentation for capillary zone electrophoresis with on-column detection

12 μm polyimide coating
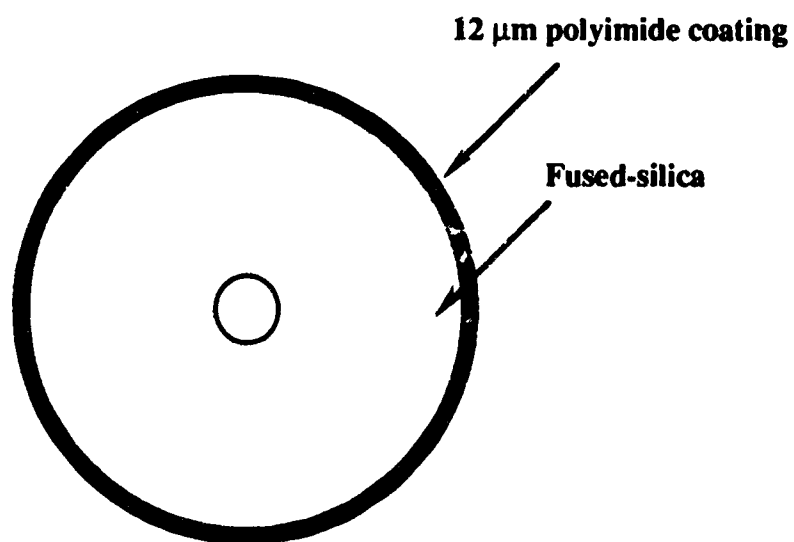
Fused-silica

Figure 1.2

Cross-section of 50 μm i.d. x 360 μm o.d. fused-silica capillary with polyimide coating

1.1.2 Advantages of capillary zone electrophoresis

The major limitation in conventional electrophoresis is the temperature rise induced by the electrophoretic current. Joule heating can result in temperature gradients. The subsequent density gradients and convection increase zone broadening, affect electrophoretic mobilities, even lead to boiling of the operating buffer. In large scale electrophoresis, a supporting medium such as gel is used to help dissipate heat, thereby minimizing zone broadening. However, the support increases the surface area for adsorption and introduces eddy diffusion. An unique advantage of capillary electrophoresis is the enhanced heat dissipation relative to the volume of operating buffer in the capillary. Heat can be only dissipated through the capillary wall. Hence, narrow bore capillaries provides larger ratio of surface area to volume. This permits the use of very high electric field which is necessary for fast and efficient separation. Other advantages of using a capillary include minimized convection due to small radius, sampling from a microenvironment like a single cell and easy automation.

1.1.3 Electroosmosis and zeta potential (ζ)

Electroosmosis is the flow of bulk solvent caused by the electrical double layer adjacent to the inner surface of capillary under the influence of an electric field. This phenomenon can be explained by the interaction of silanol group with aqueous solution at the inner wall of the fused-silica capillary. Figure 1.3 is a model of the silica-solution interface in a fused-silica capillary tube. The Si-OH group of the silica surface is ionized to Si-O⁻ in alkaline and slightly acidic media (pH > 2). Since the inner wall of capillary is negatively charged, positive counterions are present in the stagnant double layer and diffuse layer. The potential across the layers is termed zeta potential ζ, which is given by

$$\zeta = 4 \pi \eta \, \mu_{eo} / \varepsilon \qquad\qquad (1.1)$$

(a)

CAPILLARY INNER SURFACE

(b)

CAPILLARY WALL

μ_{eo}
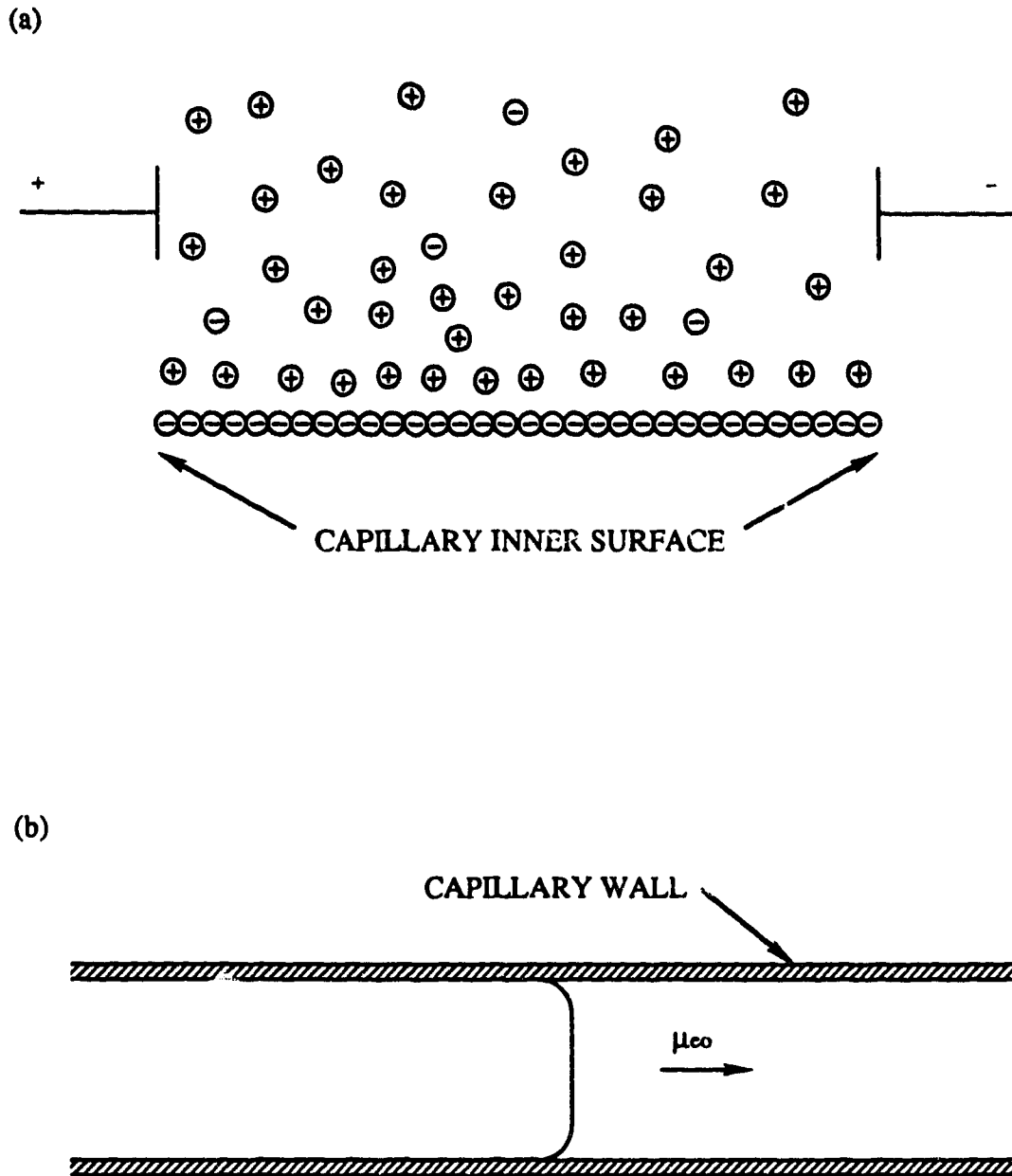
Figure 1.3 (a) Schematic representation of silica-solution interface

(b) Schematic representation of the flow profile during electroosmosis

Where η is the viscosity of the operating buffer, μ_{eo} is the electroosmotic flow coefficient, and ϵ is the dielectric constant of the carrier buffer.

$$\mu_{eo} = D \; \zeta_{eo} / 4 \pi \eta \qquad (1.2)$$

The thickness of the double layer is on the range of a few nanometers to a few hundred nanometers depending on the concentration of carrier buffer.

When an electric field is applied across a narrow bore capillary, the solvated counterions in the diffuse layer migrate with a flat flow profile towards the cathode as shown in figure 1.3 (b). The net elution rate of any charged component is the sum of the electroosmotic flow and the electrophoretic mobility of the ion. Therefore, the rate of electroosmosis flow can affect separation time and resolution (38,42). The chemical properties of the interface can also affect analyte adsorption which results in band broadening.

1.1.4 Retention Time, separation efficiency and resolution

Retention Time

Retention time t_r is the time for a solute to migrate through the entire capillary, given by:

$$t_r = L^2 / (\mu_{ep} + \mu_{eo}) V_{ep} \qquad (1.3)$$

where L is the capillary length, μ_{ep} is the electrophoretic mobility of the sample, μ_{eo} is the electroosmotic flow coefficient, V_{ep} is the applied voltage (38). It is clear that short retention time is achieved by the use of short capillary and high voltage.

Separation efficiency

Separation efficiency in terms of the total theoretical plates, N, is given by

$$N = (\mu_{ep} + \mu_{eo}) V_{ep} / 2D \tag{1.4}$$

where D is the solute's diffusion coefficient. This equation predicts that the total number of theoretical plates is proportional to the applied voltage and has nothing to do with the capillary length, thus high efficiency separations are best performed with high voltage (38). However, the applied voltage can not be increased infinitely otherwise the increasing Joule heat will become significant. The number of theoretical plates can be calculated from peak profile using the formula:

$$N = 16 (t_r / w)^2 \tag{1.5}$$

where w is the baseline peak width.

Resolution

Jorgenson and Lukacs (38) derived the equation to predict the resolution of two zones in capillary zone electrohporesis, followed the approach of Giddings (23).

$$Rs = 0.177 (\mu_{ep_1} - \mu_{ep_2}) [V_{ep} / D (\bar{\mu} + \mu_{eo})]^{1/2} \tag{1.6}$$

where μ_{ep_1} and μ_{ep_2} are the electrophoretic mobilities of the two zones and $\bar{\mu}$ is their average mobility. It is clear from equation (1.4) and (1.5) that a rapid electroosmotic flow in the same direction of electrophoresis will yield higher number of theoretical plates, but will degrade the resolution of the two zones. In other word, a fast electroosmotic flow will result in sharp but poorly resolved peaks.

1.1.5 Sample Injection

Electrokine'   d hydrodynamic injection are best suited to sample introduction into 25 - 75 μm i.u   ·illaries (38,40,63,20). They are both able to dk '.ver nanoliters of sample into the capillary reproducibly. Several other injection methods such as an electric sample splitter (15), a rotary injector (77) and a micro injection system (81,82) have been designed for 200 μm - 300 μm i.d. capillaries.

Electrokinetic Injection

In electrokinetic injection, also called electromigration injection, the anodic end of the capillary and the anode are placed into the sample vial together. 1 kV - 5 kV injection voltage is briefly applied, causing electromigration of small plug of sample into the capillary. The capillary and the anode are then placed into the buffer reservoir, and separation voltage is applied. This method of injection is quite simple and effective, introducing sample with minimal zone broadening (42). The operator is protected from electrical shock during sample injection by an interlock system, but the operator should not touch the interlock activator. The high voltage end of the electrophoretic system is enclosed in a Plexiglas box. The quantity of sample injected into the capillary can be calculated by (51)

$$Q_{inj} = (\mu_{ep} + \mu_{eo}) V_{inj} t_{inj} \pi r^2 C / L \tag{1.7}$$

where μ_{ep} is the electrophoretic mobility of the sample, μ_{eo} is the electroosmotic flow coefficient, t_{inj} is the time over which the injection voltage V_{inj} is applied, r is the inner radius of the capillary, C is the sample concentration and L is the capillary length. The capillary length L is given by

$$L^2 = (\mu_{ep} + \mu_{eo}) t_r V_{ep} \tag{1.8}$$

t_r is the retention time of the sample when the electrophoretic voltage V_{ep} is applied. The amount of sample injected can also be determined by substituting equation (1.8) into (1.7)

$$Q_{inj} = L \pi r^2 C V_{inj} t_{inj} / V_{ep} t_r \qquad (1.9)$$

The equation (1.9) tells that the drawback of electromigration injection is the discrimination for ionic components with different mobility. The positively charged component with higher mobility is introduced into the capillary faster than the component with lower mobility (32,63); neutral components are introduced by electroosmotic flow only; The negatively charged components are introduced in the smallest amounts.

Equation (1.9) or (1.7) is applicable only when the conductivity of the sample solution and the buffer are approximately equal. When the sample is not prepared in the operating buffer, electrokinetic injection is also affected by the conductivity of the sample solution (32).

Hydrodynamic Injection

In hydrodynamic injection, the end of the capillary is placed into the sample reservoir, followed by lifting the sample reservoir to a specified height which is Δh higher than the other end of the capillary for an interval of time (63). This height difference Δh causes hydrostatic pressure, pushing the sample into the capillary without any discrimination for ionic components. The quantity of sample injected can be calculated by

$$Q_{inj} = \rho g \pi r^4 \Delta h C t_{inj} / 8 \eta L \qquad (1.10)$$

where ρ is the solution density, g is the gravitational force constant, r is the inner radius of the capillary, Δh is the height difference between the liquid levels of the sample

reservoir and buffer reservoir at the grounded electrode, t_{inj} is the time of injection, η is the viscosity of the sample solution, L is the capillary length.

1.2 Detection in capillary zone electrophoresis

Capillary zone electrophoresis (CZE) has turned out to be a very powerful technique for the separation of charged species as well as neutral species. It is particularly important for the fast separation of biological macromolecules such as oligoneucleotides, proteins and DNA. However, one of the major limitation in capillary electrophoresis seems to be the lack of sensitive detection. Most detection techniques used in liquid chromatography can also be used in CZE. The construction of post-column flow cell is hardly possible in CZE if not using sheath flow cuvette because it is extremely difficult to connect the commonly used 5-100 μm i.d. capillaries with another flow cell. The coupling of another tube to the capillary will definitely result in extra band broadening which deteriorates resolution (45). Accordingly on-column, non-contact detections are used more often in CZE. Several detection techniques in CZE will be summarized below.

1.2.1 UV-absorbance

UV-absorbance detection has been used in CZE for more than one decade. On-column detection must be performed in order to minimize loss of resolution caused by detector dead volume. The construction of the on-column detector can be simply done by removing a short portion of the polyimide coating from the capillary and then placing light sensor close to the transparent capillary. According to Beer's Law, the sensitivity of UV-absorbance in CZE is dependent on the molar absorptivity of the analytes and the optical path length which equals the internal diameter of the capillary. Therefore, the sensitivity of absorbance can be adjusted by changing the internal diameter of the capillary. However, better separation is achieved with smaller i.d. capillary. Typically, concentration limit of detection is restricted to 10^{-5} M level (92). The sensitivity drops

rapidly when dealing with 10 μm or less i.d. capillaries. Although the sensitivity of UV-absorbance detection is relatively poor it has remained the most popular detection approach. The use of high power light sources like UV lasers and xenon lamps and improved optical sensors may reduce the detection limit. However, the limited range of wavelengths restrict their applicability.

1.2.2 Fluorescence

Fluorescence detection is by far the most sensitive technique in capillary electrophoresis because the analyte signal is measured against an extremely low background signal (9,10,12,38,73,91,93). The major background noise in on-column fluorescence detection is light scattering which may interfere with the fluorescence. The intensity fluctuation of excitation source can also increase background noise level, thereby reducing the signal-to-noise ratio.

On-column detection is accomplished usually by focusing the excitation source onto the capillary and collecting the fluorescence light at right angle to the incident light in order to reject stray light interference. Laser is often used as an excitation source because it is monochromatic and well collimated, thus easily focused onto small capillaries. Helium cadmium lasers seem to be the most popular (6,22,26,62,56,90), since they are not very expensive and emit in the UV range (325 nm). Argon ion lasers have also been used extensively for excitation of fluorescence in capillary electrophoresis (4, 12,13,16,72,91), since they provide higher power at 488 nm. However, it is rather expensive and requires forced air cooling. Recently, a semiconductor laser has also been used as an excitation source in capillary electrophoresis (28). This laser is good for capillary electrophoresis especially due to its low price and small dimension. Arc lamps have also been used as an excitation source, where the excitation wavelength can be selected with optical filters (38,40,51).

The post-column laser-induced fluorescence detection via a sheath flow cuvette presented the best detection limit in CZE (10). Detection limit of 30 analyte molecules have been produced with this technique. In this detector, the outlet of capillary is inserted into a 200 μm square quartz flow chamber. The sample flows as a narrow stream surrounded by a sheath stream consisting of the same buffer as that used for electrophoretic separation. The high quality windows of the cuvette produces at least two orders of magnitude less light scattering than an on-column detector.

The inevitable disadvantage of fluorescence detection is pre-column labeling of the non fluorescent sample molecules, which is usually required since very few molecules fluoresce.

1.2.3 Radioisotope

Radioisotope detection is not frequently used in CZE. Altria et al. provided the earliest detection of radio pharmaceuticals containing radioactive technetium in CZE (3). Pentoney, Zare and Quint have made an on-column detection of ^{32}P-labeled molecules by placing a semiconducting CdTe wafer near the outlet of the capillary as a radioactive detector (59,60). They were able to obtain detection limit of 100 attomoles for ^{32}P-labeled ATP.

1.2.4 Mass Spectroscopy

Capillary zone electrophoresis has been coupled to a mass spectrometer through an electrospray-ionization (ESI) interface by Smith and co-worker (48,49,58,67-70,78). The interface was based upon direct electrospray ionization from the terminus of the capillary. The key of CZE-MS interface is the excellent electrical contact of the electrophoretic buffer at the capillary outlet. This was made by either a small needle (58) or a vapor deposited silver coating on the capillary exit included by a stainless steel tubing (67). This electrical contact was also used to provide ESI voltage which was

typically 3 ~ 5 kV. The focusing electrode was typically at 300 V, while the sampling nozzle and skimmer are at ground potential. The ESI ion source functions at atmospheric pressure. The cloud of electrospray was desolvated by the hot N_2 curtain before the ions entered the quadruple mass spectrometer. Although the ESI process has not been understood very well it has been found that buffer composition, pH, desolvation gas flow, electric field strength and even analyte concentration can be important variables for ESI mass spectra. Detection sensitivity and resolution vary widely as well (67). CZE-MS provides detection limit in femtomole range, more than 10^5 theoretical plates and structural information for many compounds.

1.2.5 Amperometry

The first post-column amperometric detection in CZE was made by Wallingford and Ewing (81-86). They used a porous glass joint to connect the separation capillary with detection capillary to make an electrical contact with the electrophoretic buffer prior to detec. on spot. A 5-10 μm o.d. carbon fiber electrode was inserted into the capillary. This joint was immersed in the buffer reservoir that contains the ground electrode. The electroosmotic flow from the first capillary is able to pass through this joint to the carbon-fiber electrode located at the end of second capillary. This porous glass joint serves as a ground to complete the electrophoretic circuit, thus isolating the amperometric detector from the high voltage. The authors reported detection limits of 200-400 attomoles for catecholamines separated in a 26 μm i.d. capillary.

1.2.6 Conductivity

Conductivity detection has been used in ion chromatography for almost two decades. As a universal detector, it is less sensitive than the specific detector which responds only to the analtye molecules. The commonly used capillaries have internal diameter as small as 10 ~ 100 μm. The construction of conductivity detector with low

dead volume in CZE is extremely challenging. Huang and Zare have pointed out the three possible designs, on-column, end-column and post-column structures for a CZE conductivity detectors (37). In 1979, Mikkers described the first conductivity detection in CZE (54,55). In 1985, Deml et al. employed conductivity detection (15). In 1986, Foret et al. constructed an on-column conductivity detector which consisted of three ium wires cast into a polyester resin block attached to the cathodic end of the separation capillary (19). In 1987, Huang et al. described the most versatile on-column conductivity detector in CZE (30). A computer-controlled CO_2 laser was used to punch two 40 μm holes on the opposite sides of 50 μm i.d. or 75 μm i.d. capillary. Two 25 μm diameter platinum wires were inserted into these holes and sealed with epoxy adhesive as sensing electrodes. The electrodes must be placed horizontally across the capillary in order to minimize the interference from high electric field. The electric field in CZE is usually 200 ~ 300 V / cm, an ac conductivity circuit with isolation transformer must be used to measure the conductance (17,30). Detection limit was 10^{-7} M for Li^+. Low molecular weight carboxylic acids have also been detected with this conductivity detector (31). Private correspondence with the author tells that this technique is not easy. In order to avoid the high electric field, Huang and Zare designed an end-column conductivity detector in 1991 (36,37). In this detector, a 60 μm hole was punched by CO_2 laser 7 mm from the outlet of the 75 μm i.d. x 363 μm o.d. capillary. A 50 μm diameter platinum wire was then inserted into the capillary until it just reached the hole. The end-column conductivity detector was found to give rise to 17% extra band broadening compared with on-column conductivity detector. The conductivity was measured between the 50 μm sensing electrode and the grounding electrode. They proved that the concentration of buffer in the ground reservoir does not affect sensitivity, but the buffer inside the capillary does affect the sensitivity significantly. Post-column conductivity detectors may be constructed by grounding the capillary prior to the sensing electrode, using either a porous glass structure (83) or an on-column frit structure(33).

Conductivity signal often shows a poor reproducibility and time dependent instabilities, which are not of electronic origin (79). Baseline drift, signal wander and ghost peaks are the major problems in conductivity detection. These unwanted phenomena are primarily due to electrochemical effects, adsorption and the existence of impurities. Temperature drift has only a minor influence.

Conductivity detection functions in displacement mode. When an analyte ion of the same charge as that of the buffer ion is injected, there is a one to one displacement of the buffer ion with same charge in the sample zone to maintain constant ionic strength. The displacement of the buffer ion results in a increase or decrease of the background signal depending upon the difference of conductivity between the analyte and the buffer.

1.2.7 Chemiluminescence

Based on the luminol-hydrogenperoxide reaction, Dadoo, Colon and Zare described the first chemiluminescence detection in capillary electrophoresis (14). The electrophoretic capillary (75 μm i.d. x 375 μm o.d.), reagent capillary (200 μm i.d. x 375 μm o.d.) and reagent capillary (150 μm i.d. x 375 μm o.d.) were held together by a PEEK tee connector. The reagent capillary is used to deliver the catalyst solution to react with luminol eluted from the electrophoretic capillary. A 3-4 cm section at the end of the electrophoretic capillary was eched to approximately 100-120 μm outer diameter and inserted into the reaction capillary. A 2-3 mm detection window was made by burning off the polyimide coating on the reaction capillary. It was placed at the focal point of a parabolic reflector. The other part of the reaction capillary was painted black to prevent residual light emission after the detection window from reaching photomultiplier tube (PMT). The collimated light from the reflector was then focused by a planoconvex lens onto the PMT which was cooled to - 20 °C to reduce dark current. On-column luminol chemiluminescent reaction provides sensitivity several orders of magnitude greater than UV-absorbance due to the low background noise. Detection limit is 3 x 10^{-9} M level for

luminol and 7 x 10^{-9} M for N-(4-aminobutyl)-N-ethylisoluminol (ABEI). However, the peak width is very broad (one minute).

1.3 Comparison of capillary ion analysis and ion chromatography

Ion chromatography (IC) is a separation technique developed in 1975 (66). Since then it has grown quickly and become a routine separation method in many areas. Recently, it encounters a challenge from capillary ion electrophoresis (CIA) created in 1991 by Waters (53,11,25,27,45,61,64,89). Waters claimed that CIA is " a revolutionary advance over conventional ion chromatography " because CIA can separate a mixture of 30 standard anions in three minutes which is nearly 10 times faster than conventional chemically suppressed IC. Waters says this new technology also offers the analyst better separation efficiency and resolution. Compared with the average 2000 theoretical plate efficiency of suppressed IC, CIA often generates 500,000 plates which translates into a large increase in resolving power for ionic species. This high separation efficiency and fast speed can be hardly achieved by any other separation schemes. Indirect UV detection is generally employed in CIA. Detection limit is up to part-per-billion range.

CIA separates ionic species based on the difference of ionic mobility rather than ion exchange mechanism. A UV-absorbing substance is added to the buffer to generate a high background signal. To achieve a maximum signal-to-noise ratio, the UV lamp must be extremely stable. When high voltage is applied, the ions will migrate differentially along the capillary. Many sample zones are formed. In order to keep the constant ionic strength, some UV absorbing additive is replaced by the analyte, producing a negative peak which is proportional to the analyte concentration. This indirect detection scheme measures small changes against a large background signal.

1.4 Conductance and mobility of ions

1.4.1 Conductance

The conductance of an electrolyte is the reciprocal of the resistance R and expressed:

$$1 / R = \kappa (A / l)$$

<div align="right">(1.11)</div>

where κ is the specific conductance or conductivity in units of S / m; A is the area of the electrolyte and l is the length of the electrolyte. The ratio l / A for a conductimetric cell is known as the cell constant. Conductivity is the reciprocal of resistivity, it is a function of the concentration of the electrolyte. For very dilute solutions of strong electrolytes, the conductivity is proportional to concentration. The equivalent conductance, Λ, is defined as the conductance of a volume of solution containing one equivalent weight of dissolved substance when placed between two parallel electrodes 1 cm apart, and large enough to contain all the solution between them (88). Λ is never determined directly, but calculated from the specific conductance. It is related to specific conductance and concentration, C, in gram equivalents / l as follow (50):

$$\Lambda = 1000 \, \kappa / C$$

<div align="right">(1.12)</div>

The unit for Λ is S x m^2 / equiv. The analyte concentrations normally encountered in capillary zone electrophoresis are below the millimolar level which is low enough for Λ to be independent of concentration. At infinite dilution, Λ is called limiting equivalent conductance, Λ^o.

1.4.2 Mobility

The mobility of an ion at any finite equivalent concentration is the velocity with which the ion moves under unit potential gradient (88). Its unit is $m^2 / (s\ V\ equiv.)$. At infinite dilution, the ionic mobility reaches a limiting maximum value called absolute mobility, $\mu^o (m^2 / s\ V)$. The absolute mobility μ^o is related to the limiting equivalent conductance Λ^o of the ions:

$$\mu_+^o = \Lambda_+^o F \qquad\qquad\qquad \mu_-^o = \Lambda_-^o F \qquad\qquad (1.13)$$

where F is the Faraday constant (96485.309 coulombs). At finite concentration, values of $\Lambda_\pm$ are substituted for $\Lambda_\pm^o$, and ionic mobility decreases with increasing concentration. The absolute mobility of an individual ion can be calculated from its limiting equivalent conductance.

CHAPTER II

THE APPLICATION OF MICRO-MACHINING TECHNOLOGY FOR
THE CONSTRUCTION OF END-COLUMN CONDUCTIVITY
DETECTOR IN CAPILLARY ZONE ELECTROPHORESIS

2.1 Instrumentation

Figure 2.1 (a) shows the overall instrumentation for end-column conductivity detection in CZE. The detection spot is located inside the ground buffer rather than on-column as shown in figure 1.1. The entire CZE system was constructed on a well-damped 4 x 8 feet optical breadboard (Newport). A high voltage d.c. power supply (Spellman) provides a variable voltage of 0 ~ 30 kv to drive the electrophoresis. For safety purpose, the high voltage end of the CE system is enclosed in a 40 cm x 20 cm x 30 cm Plexiglas box with interlock system which is able to disconnect the high voltage in case the Plexiglas box is accidentally opened. Electrophoresis was performed in 52 μm i.d. x 360 μm o.d. x 40 cm long fused-silica capillary with polyimide coating. A 1.5 ml plastic vial is placed at the high voltage end of the capillary as buffer reservoir. A rotating Plexiglas holder was used to adjust the plastic vial up and down during the sample injection. The conductivity detector holder was immersed about 5 cm in the buffer. A 25 ml buffer reservoir at grounding end is used to reduce the temperature fluctuation since no thermostating device was used in the experiment. Parafilm is used to cover this reservoir to prevent the external dust from sneaking into the reservoir. The Araldite epoxy provided a good sealing at the end of the Plexiglas tubing. To eliminate siphoning effect, a small lab jack is used to adjust the liquid level of the ground buffer equal to that of the same buffer at the high voltage end. The ground electrode is a 0.8 mm diameter x 6 cm long platinum wire which was soldered to a coaxial cable. The other end of the coaxial cable is connected to the electronic circuit for conductivity detection via. a BNC connector. Figure 2.1 (b) shows the configuration of the end-column conductivity detector in detail.

(a)
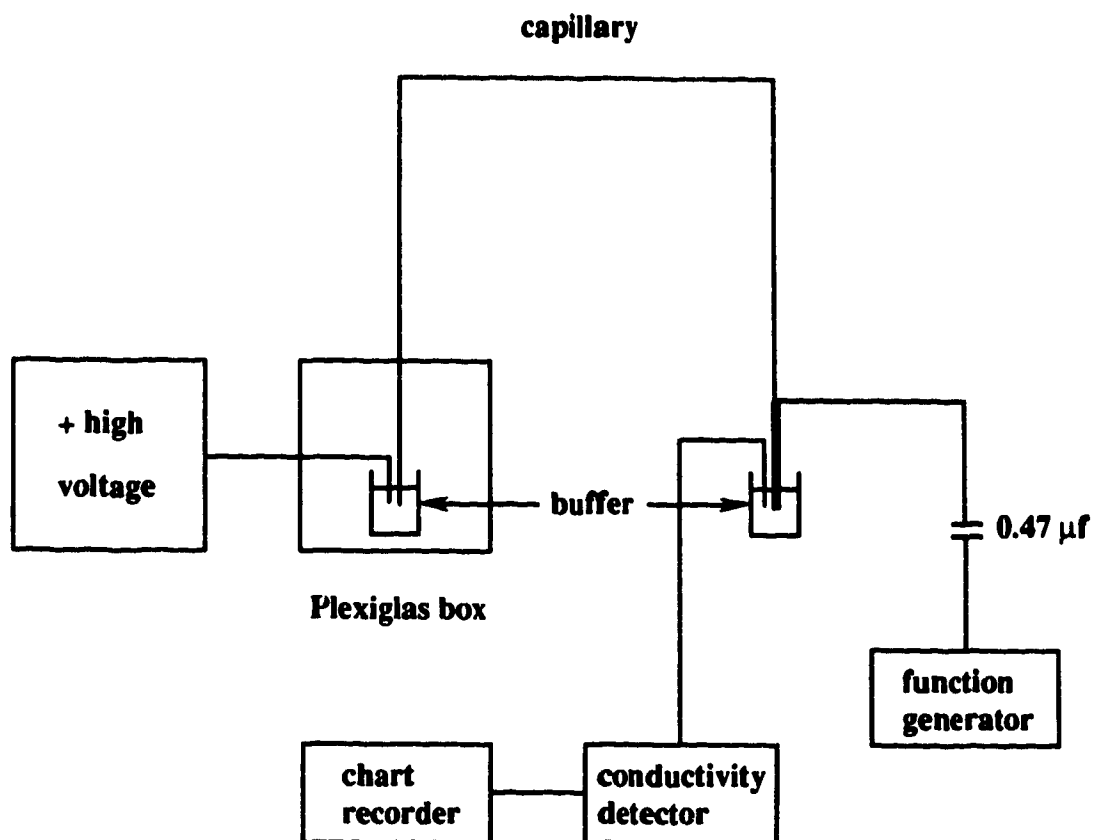
Figure 2.1

Instrumentation for end-column conductivity detector in capillary zone electrophoresis

Capillary: 40 cm x 52 μm i.d. x 360 μm o.d.; slit size: 55 μm wide x 164 μm deep

Platinum electrode: 15 mm long x 50.8 μm diameter

(b)

52 μm i.d. x 360 μm o.d.
fused-silica capillary

conductivity detector

0.47 μf capacitor

fuction generator

coaxial cable

1/8" i.d. x 1/4" o.d.
Plexiglas tubing

25 ml ground buffer

epoxy
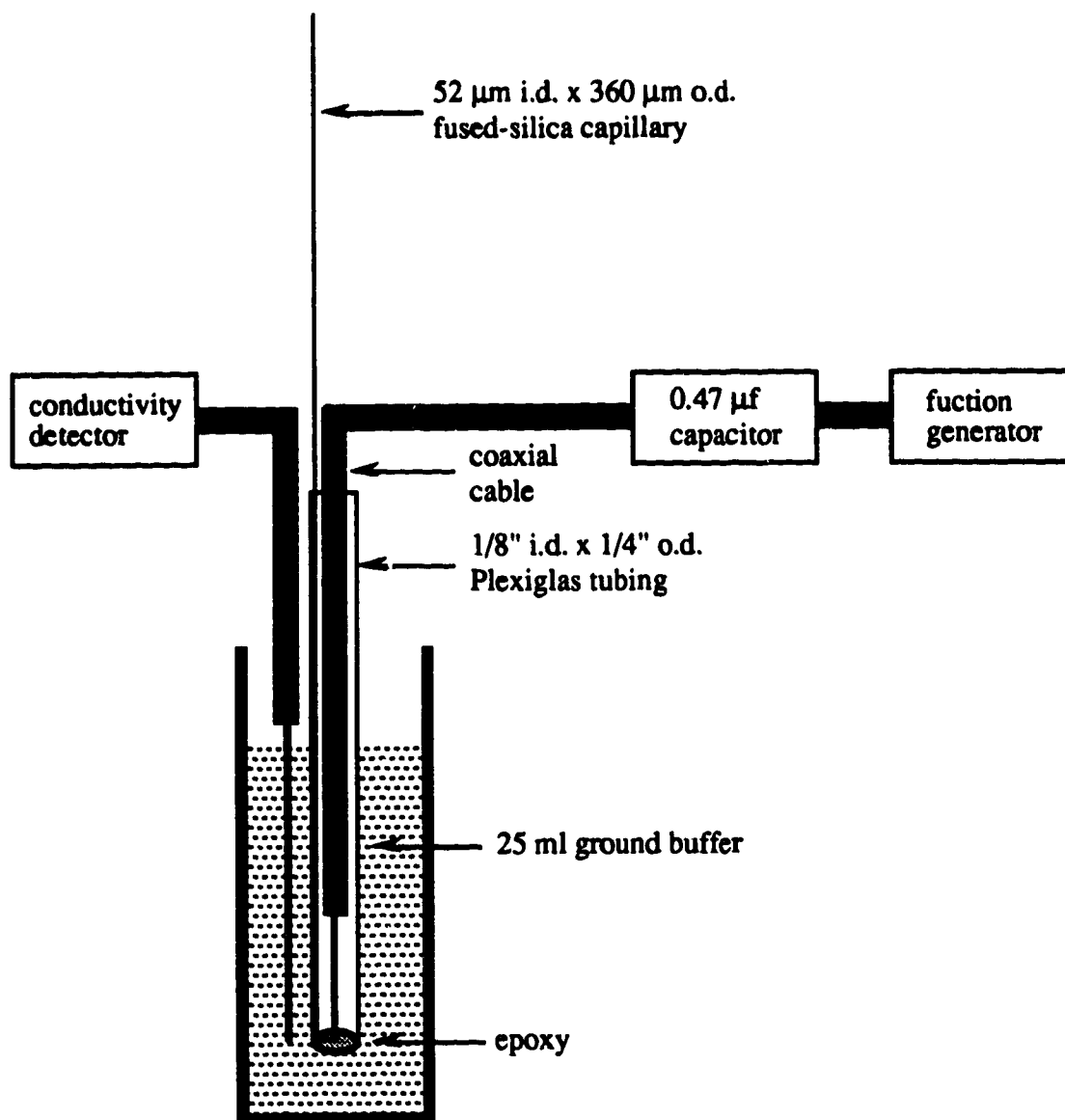
Figure 2.1 (continued)

Instrumentation for end-column conductivity detection in capillary zone electrophoresis

Capillary: 40 cm x 52 μm i.d. x 360 μm o.d.; slit: 55 μm wide x 164 μm deep

Platinum electrode: 15 mm long x 50.8 μm diameter.

2.2 Reagents

1. Lithium Chloride (anhydrous) 99.99% [7447-41-8]

   LiCl = 42.39

   Aldrich Chemical Company, Inc.

2. Sodium Chloride 99.999% [7647-14-5]

   NaCl = 58.44

   Aldrich Chemical Company, Inc.

3. Potassium Chloride 99.99% [7447-40-7]

   KCl = 74.56

   Aldrich Chemical Company, Inc.

4. Rubidium Chloride (Purified)

   RbCl = 120.92

   Fisfer Scientific

5. MES (2-[N-Morpholino]) ethanesulfonic acid [4432-31-9]

   FW = 195.2

   Lot 40 H5601 M8250

   Sigma Chemical Co.

6. L-histidine [71-00-1]

   FW = 155.16

   Aldrich Chemical Company, Inc.

7. powder and liquid of Dura Lay

   Reliance Dental mfg, co., Worth, Ill, U.S.A.

2.3 Solution preparation

2.3.1 Preparation of buffer

The distilled deionized water was prepared from an ultrapure water system (Model No. 04751, Barnstead, Iowa, U.S.A.) and degassed for 30 minutes before use. MES and histidine were weighed in a 100 ml volumetric flask on a top-loading balance. They were diluted to 0.2 M as stock solution. The solution was further diluted to 0.020 M MES / histidine buffer and then filtered and degassed for about 10 minutes with 500 ml Nalgene disposable filterware. The pH of 20 mM MES / histidine buffer was measured to be 6.15 with Fisher Scientific pH meter 15.

2.3.2 Preparation of standards (0.1000 M)

LiCl, NaCl, KCl and RbCl were dried at $130^{\circ}C$ in the oven for 24 hours to remove the absorbed water. They were cooled for about 20 minutes after being removed from the oven. Exact amounts of each sample was then weighed in 100 ml volumetric flask on an analytical balance (Sartorious Research R200D). The distilled deionized water was prepared from an ultrapure water system (Model No. 04751, Barnstead, Iowa, U.S.A.) and degassed for 30 minutes before use. Then cationic standards were dissolved overnight and diluted to mark. The standards were filtered through 110 ml Nalgene disposable filterware with a 0.2 μm membrane. These standard solutions were then transferred into a 250 ml plastic bottle as stock solution. 100 μl of each 0.1 M stock solution was pipetted into a 1.5 ml plastic vial, 900 μl of 20 mM MES / histidine buffer was added to prepare 0.01 M standard solution. They were further diluted to 0.001 M in 10 ml plastic vial with 20 mM MES / histidine buffer (pH = 6.15) for future use.

2.4 Equipment

2.4.1 Capillaries

The 52 μm i.d. x 360 μm o.d. fused-silica capillaries with polyimide coating were purchased from Polymicro Technologies Inc., Arizona, USA.

2.4.2 Blade

All blades were purchased from Thermocarbon Inc., P. O. Box 181220, Casselberry, Florida, USA. Tele: (407) 834-7800.

In the present experiment, a 1.9 mil thick resin blade (Part# 2.187-1.9A-22RU7-3, Lot# E0705922235RU7-3) was used for cutting the capillary. The actual thickness of this blade was measured to be 48 μm with an ONO SOKKI digital micrometer at Alberta Microelectronic Centre.

2.4.3 Platinum wire

The 50.8 μm diameter platinum (99.99 %) was purchased from Johnson Matthey Catalog Company, 30 Bond Street, Ward Hill, MA 01835. It was used as the sensing micro-electrode for the conductivity detection in capillary zone electrophoresis.

2.4.4 Model 1100 wafer dicing saw

The micro automation model 1100 wafer dicing saw is a microprocessor-controlled, programmable, automatic saw for cutting semiconductor wafers and other hard materials (95) . The saw uses a closed circuit TV system with split image optics to align the wafer before cutting, program and data display, and monitoring. A high torque air bearing motor with controllable speed turns the cutting wheel, which accepts any two-inch nominal saw blade. Vacuum holds the wafer on the chuck while cutting. The chuck moves right, left, up and down, and rotates under operator or program control.
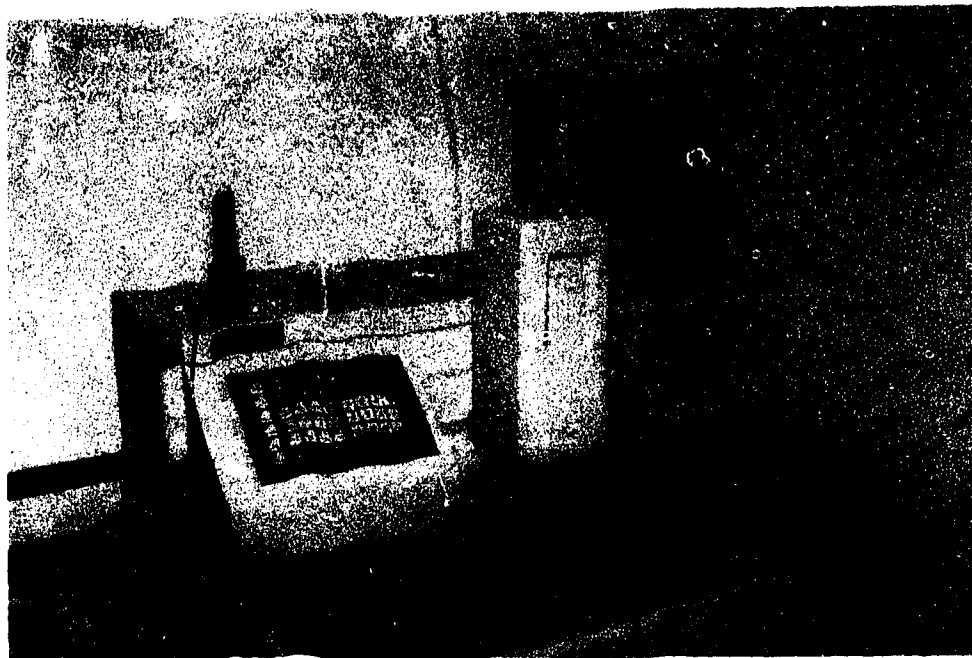
Figure 2.2

Model 1100 wafer dicing saw, Micro Automation Inc.
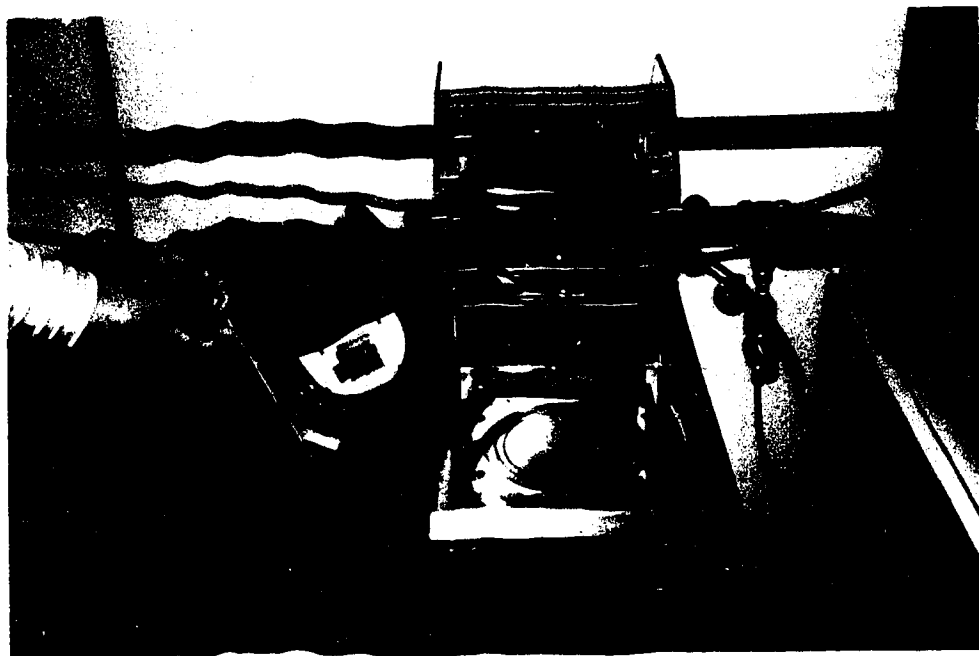
Figure 2.3

Model 150 mounting station, Micro Automation Inc.

2.4.5 Mounting Station

Figure 2.5 is the picture of Model 150 mounting station which was used to fix the capillaries onto the mounting tape (also called medium tack blue tape). This tape was purchased from Semiconductor Equipment Corp., 5154 Goldman Avenue, Moorpark, CA 93020-0779. Detailed information of the mounting tape is described in Appendix 3.

2.5 Mounting

2.5.1 Horizon ... mounting

This simplest mounting method is ideal for the radial dicing of the capillaries. The mounting frame was covered smoothly by the blue tape. The blue tape was pressed and the unwanted part was cut off along the presser. The mounting frame was then removed and Micro Automation Mounting Station was turned on. The capillaries were placed side by side on a 25mm x 75 mm microscope slide. The blue tape was used to hold all the capillaries in right angle to the edge of mounting frame. The mounted capillaries were baked on the mounting plate at about 60 °C for 10 minutes so that the capillaries were well stuck to the blue tape. The mounting frame was removed and cooled.

2.5.2 Vertical mounting

This mounting method is for the longitudinal dicing of capillaries. Dozens of 75 μm i.d. x 363 μm o.d. x 20 mm long capillaries were glued to 50 mm x 20 mm x 20 mm Plexiglas block with very small amount of Araldite epoxy (Ciba-Geigy Plastics, Duxford, Cambridge, CB2 4QA) and left for 24 hours.

The Micro Automation Station was turned on. The mounting frame was placed on top of the mounting plate. When the plate reached about 60 °C, the mounting tape was pulled onto the plate smoothly. The Plexiglas block was pressed against the tape, the mounted capillaries were baked in the oven at 80 ~ 90 °C for 10 minutes until the

Plexiglas block is well stuck to the blue tape. Care should be taken because higher temperature shrinks the tape. The mounted capillaries are removed from the oven and allowed to cool.

2.6 Dicing

2.6.1 Alignment

The ALIGNMENT was pressed, a SINGLE-CUT was made on the unwanted part of capillary. The cursor on the TV monitor was moved up and down until the cut is located exactly on the centre of the cursor, the cursor width was adjusted equal to that of the cut. The cursor must not be readjusted during the dicing process unless other cutting is on different height.

2.6.2 Radial cutting

Radial cutting is the most important section for the construction of end-column conductivity detector in CZE. The 48 μm thick resin blade (Thermocarbon Inc., Casselberry, Florida, USA) was used in all cases. By programming the wafer dicing saw, the cutting depth can be easily controlled. The wafer dicing saw must be zeroed before cutting. This can be accomplished simply by the following procedure:

Press SPINDLE ON, wait until the light stops flashing. Flush the resin blade for a few minutes, then press CHUCK ZERO. This initiates an automatic chuck zero sequence: the chuck is moved under the dicing blade on the spindle; it is raised until the chuck zero circuit detects " contact " and chuck zero is established. The indicator lamp of the CHUCK ZERO key blinks during this process, then stays lit when the chuck zero sequence is completed. The height in the program is from the top of the chuck to the bottom of the cut. The thickness of the mounting tape is measured to be 76 micrometer.

The light source from the image optics was found not strong enough to provide a clear imaging of the capillaries on the TV monitor. A flashlight was used to illuminate the capillaries to achieve a clear imaging for the alignment. This step is particularly essential for longitudinal cutting. The 2.5.2 horizontal mounting procedures were followed to mount the capillaries onto the blue tape. Install the mounting frame onto the chuck of wafer dicing saw. Press the WAFER LOCK, vacuum was applied to suck the frame tightly. The blade will be flushed as soon as dicing is started. The end of the capillaries were cut neat with a SINGLE-CUT mode. The various work being done was fully described at the bottom of each microscope picture. The edge of narrow blade is usually convex, therefore the cut on the capillary is concave at the bottom.
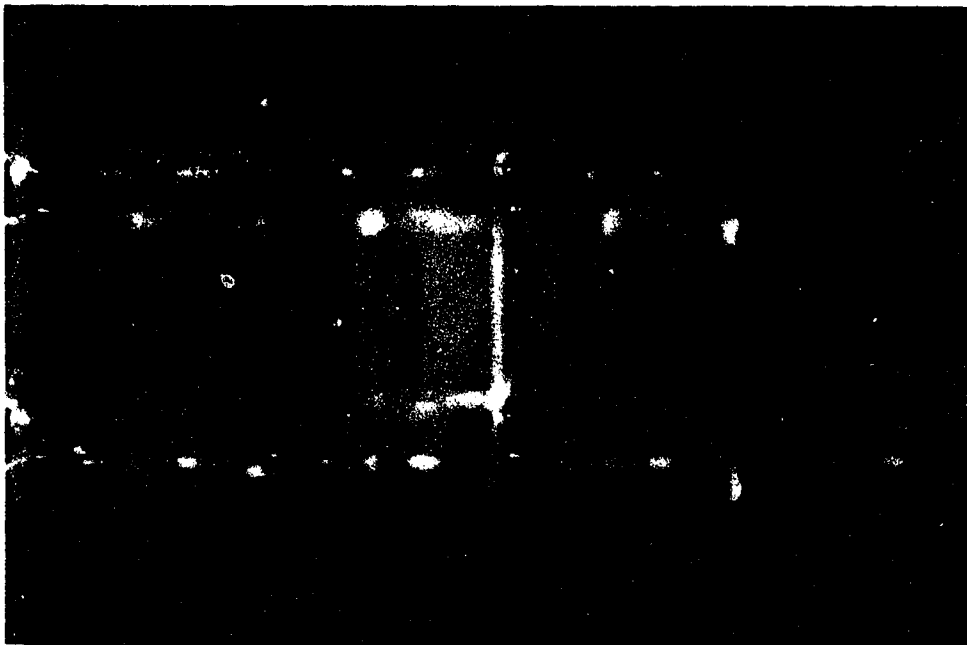
Figure 2.4

Two consecutive 105 μm deep x 55 μm wide slits with 145 μm spacing were cut radially on thirty 50 μm i.d. x 184 μm o.d. capillaries with 48 μm thick resin blade.

Top view
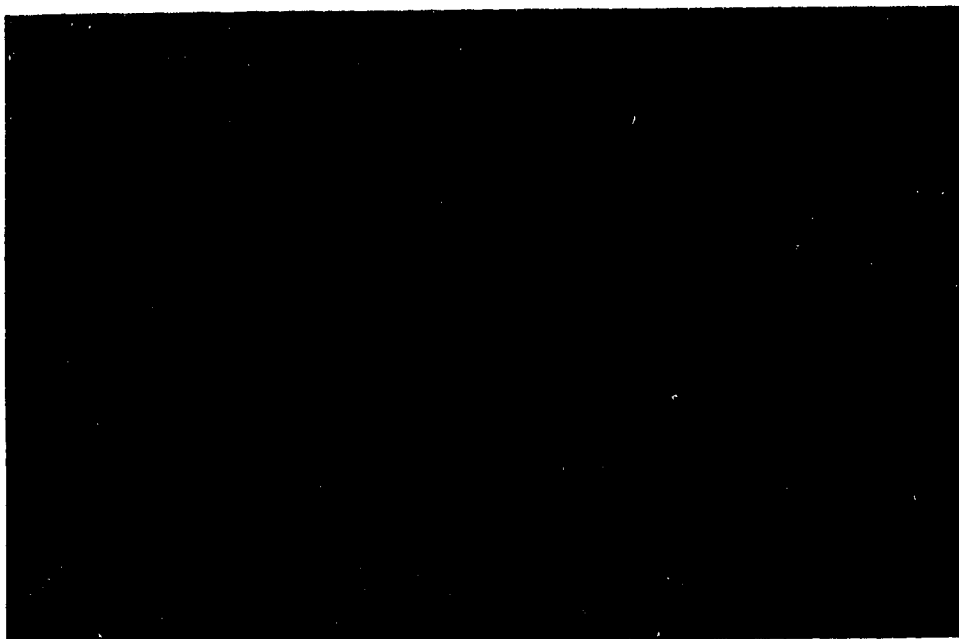
Front view
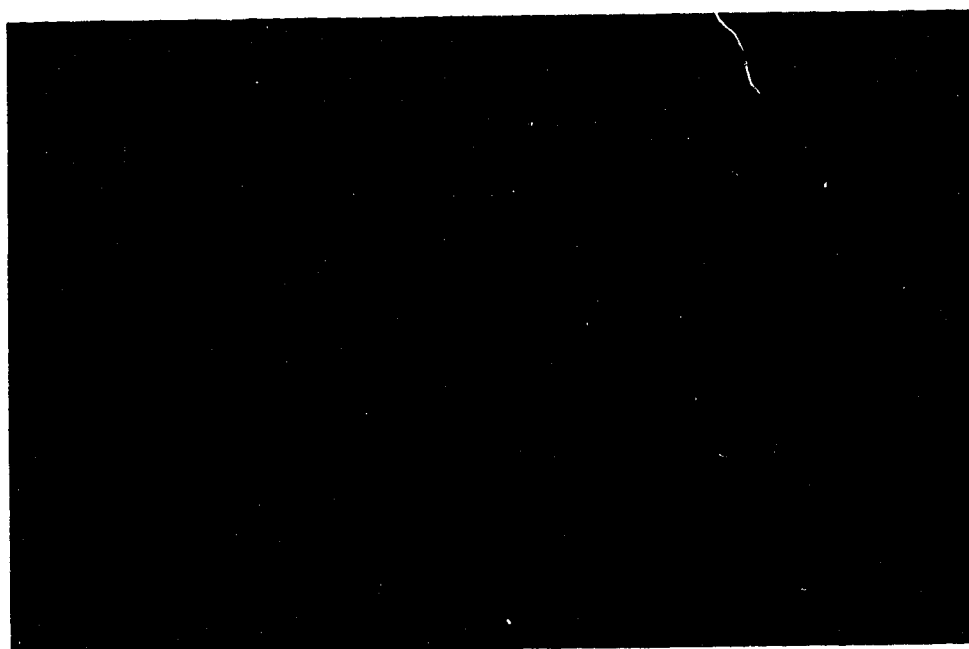
Figure 2.5

80 μm deep x 55 μm wide slit was cut radially on the 50 μm i.d. x 184 μm o.d. capillary
with 48 μm thick resin blade

Top shoot

Bottom shoot
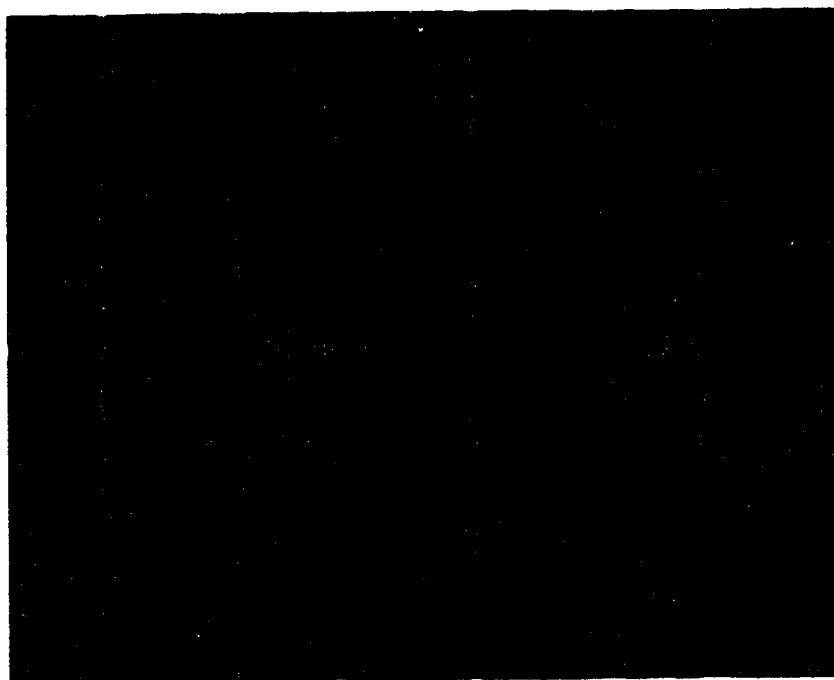
Figure 2.6

164 μm deep x 55 μm wide slit was cut radially on fourty 52 μm i.d. x 360 μm o.d. capillaries with 48 μm thick resin blade.
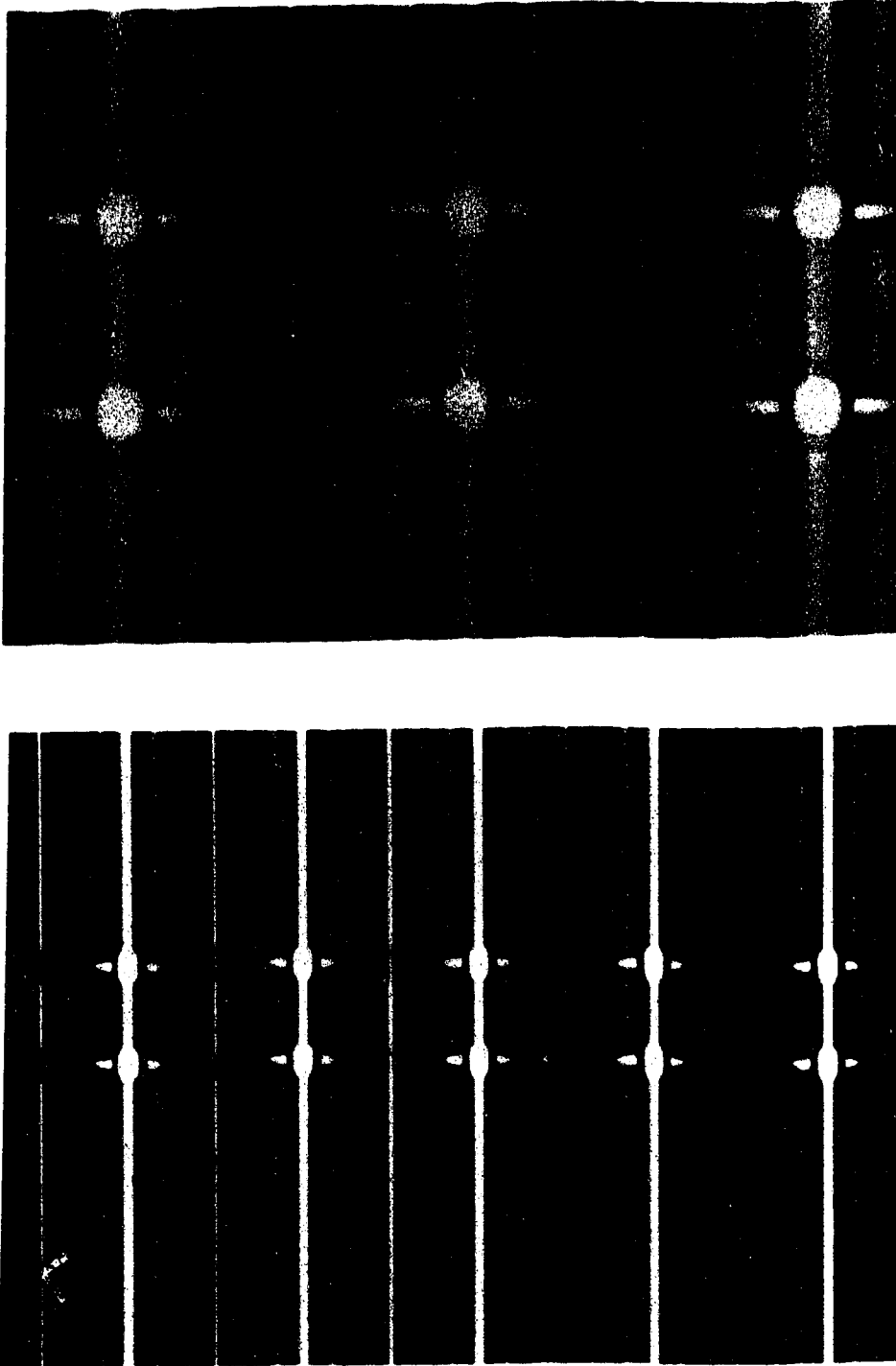
Figure 2.7

Two consecutive 160 μm deep x 55 μm wide slit with 150 μm spacing were cut radially on the 75 μm i.d. x 363 μm o.d. capillary with 48 μm thick resin blade

2.6.3 Longitudinal cutting

Longitudinal cutting is perhaps the best example to reflect the cutting accuracy of wafer dicing saw. It is hardly possible to machine a narrow slit with controllable depth and width by any other technology except wafer dicing saw. The wafer dicing saw makes this sophisticated work easy because you can almost see the result before it is done. You can see the place where you want to cut from the TV monitor.

The 50 μm i.d. x 184 μm o.d. capillary, 75 μm i.d. x 363 μm o.d. capillary and 97.6 μm i.d. x 231.3 μm o.d. capillary were used as an example to show the versatility of wafer dicing saw for logitudinal cutting on the capillaries. These capillaries were mounted vertically on the Plexiglas block described in 2.5.3 vertical mounting. The detailed work is described at the bottom of each figure.
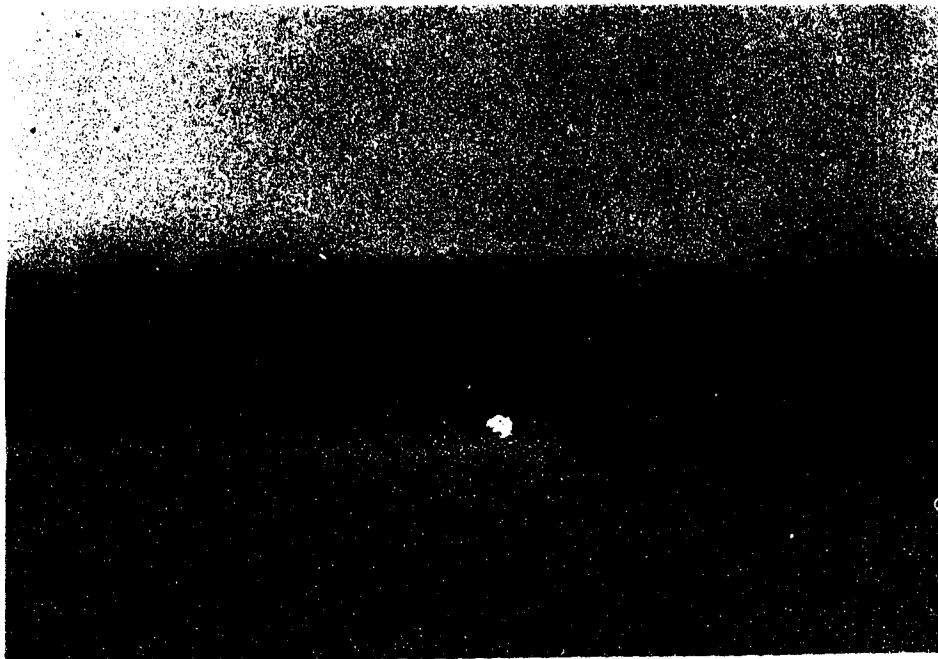
Figure 2.8

40 μm deep x 55 μm wide slit was cut longitudinally on the centre of the internal hole of 97.6 μm i.d. x 231.3 μm o.d. capillary with 48 μm thick resin blade
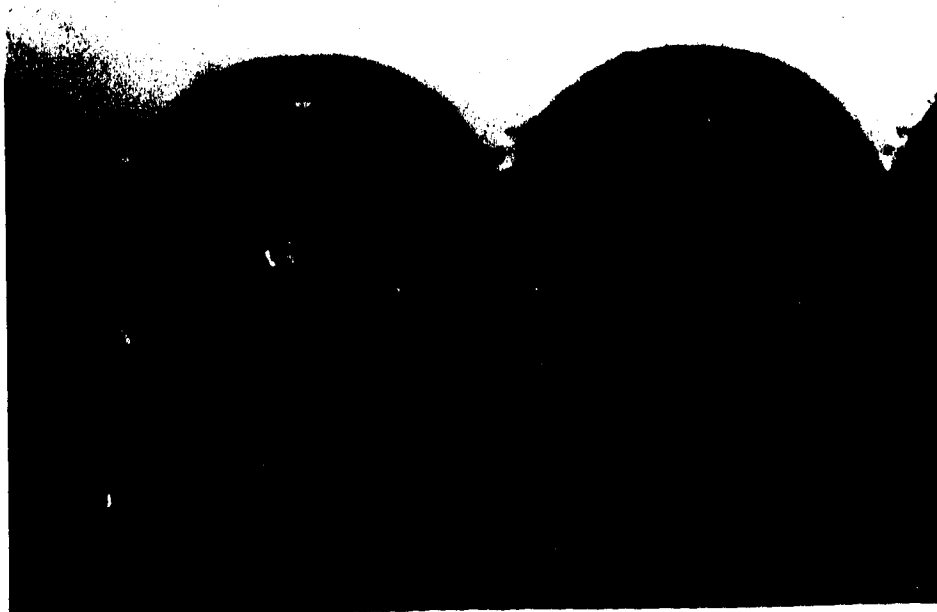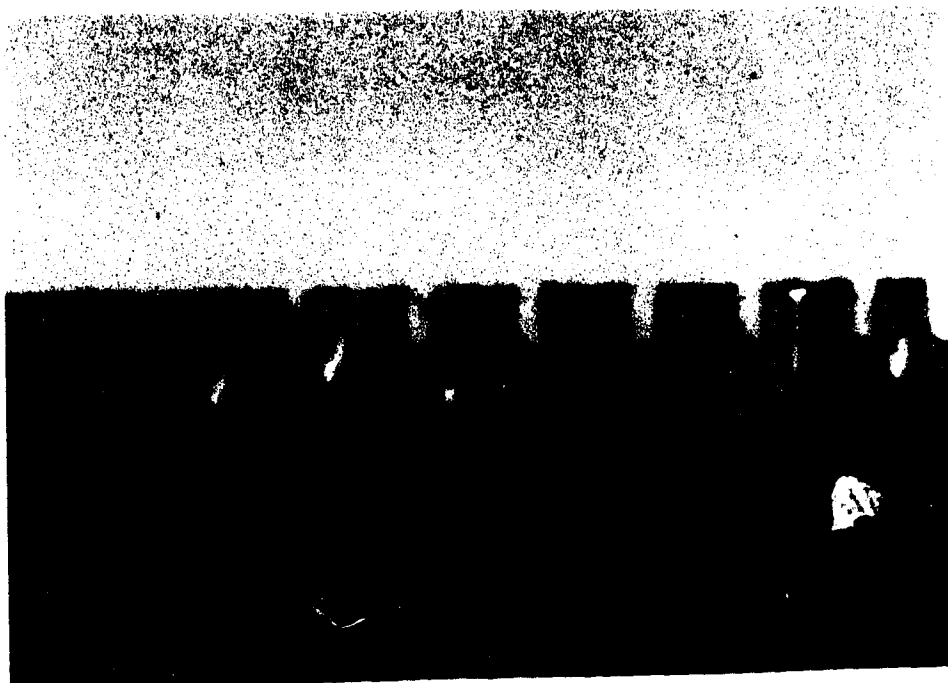
Top view

Front view

Figure 2.9

10 μm deep x 55 μm wide, 40 μm deep x 55 μm wide and 110 μm deep x 55 μm wide slits were cut longitudinally on the internal hole of the 50 μm i.d. x 184 μm o.d. capillary with 48 μm thick resin blade.

Top view
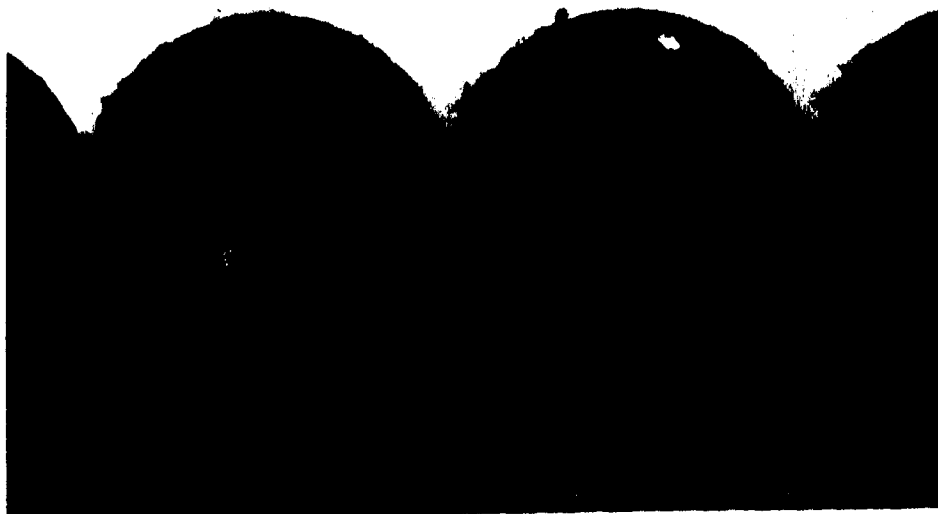
Front view
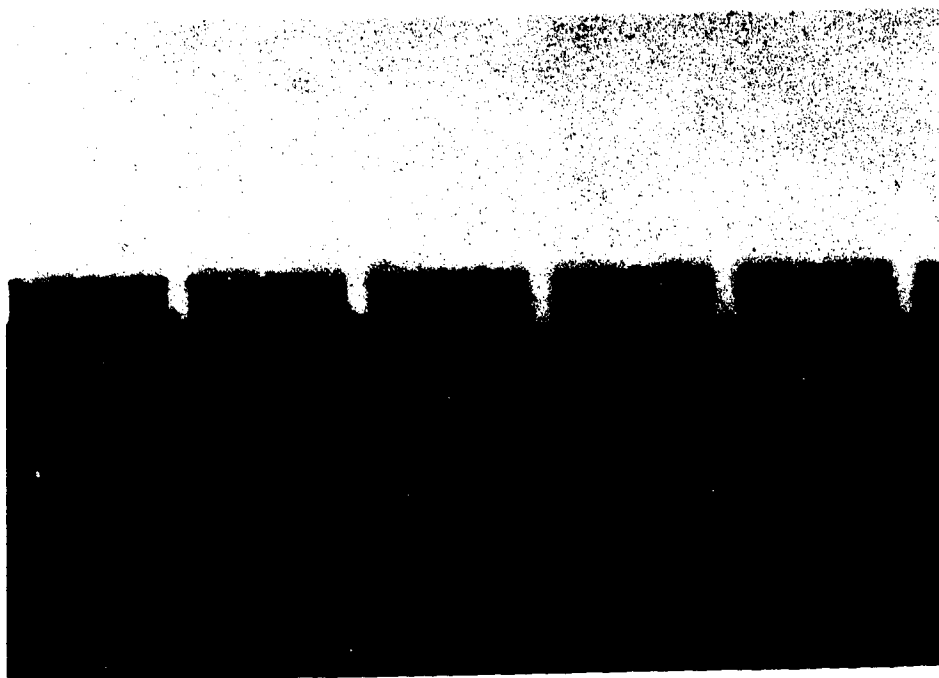
Figure 2.10

110 µm deep x 55 µm wide slits and 140 µm deep x 55 µm wide slits were cut longitudinally on the centre of the internal hole of the 75 µm i.d. x 363 µm o.d. capillary with 48 µm thick resin blade.

2.7 Making holes on capillary

The wafer dicing saw has demonstrated a versatility in the area of micro machining. A surprising way of making holes on the fused-silica capillary was developed based on the longitudinal cutting of the capillaries. First, the 75 μm i.d. x 363 μm o.d. capillary with 110 μm deep x 55 μm wide slits on figure 2.10 was removed from the Plexiglas block. Secondly, this capillary was aligned perfectly with another 75 μm i.d. x 363 μm o.d. capillary with flat cross-section, along a 300 μm deep x 370 μm wide flat-bottom channel on Pyrex plate under microscope. Thirdly, the joint of the two capillaries was melted by a micro torch under microscope. Figure 2.11 is the picture of the two holes on the capillary. The temperature of the micro torch can be adjusted near the softening point of fused-silica (1300 °C) by controlling the flow rate of acetylene and oxygen. In order to further confirm the internal hole of the capillary was not clogged, water was injected from one end, and it passed through the two holes!
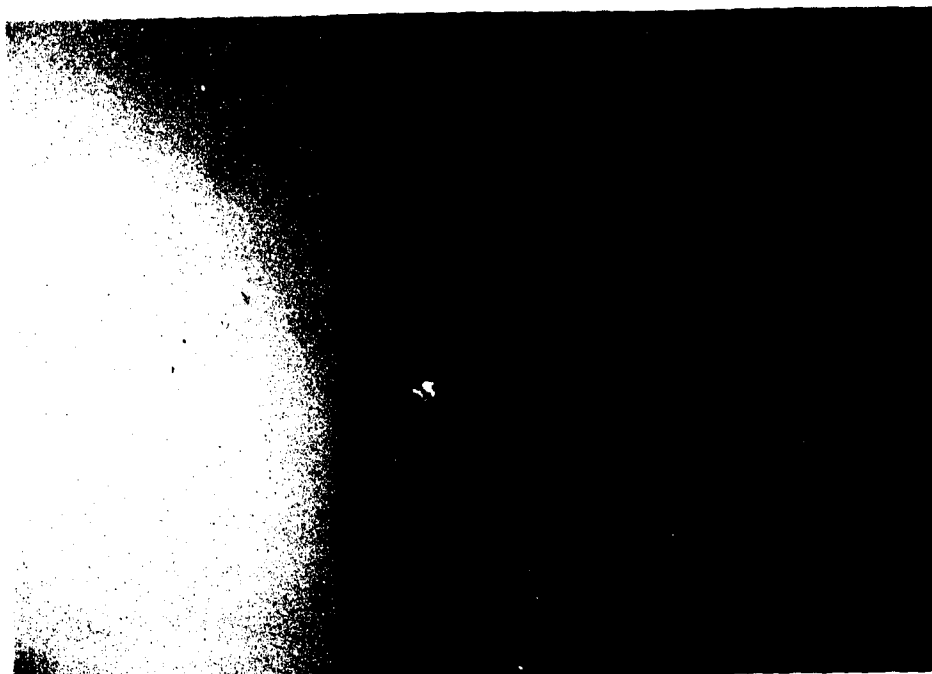
Figure 2.11
Two 110 μm deep x 55 μm wide holes were made on 75 μm i.d. x 363 μm fused-silica capillary

2.8 The advantages of wafer dicing saw over CO_2 laser

(1) Model 1100 wafer dicing saw makes narrow slits on many fused-silica capillaries with the size accurately controlled. 20 ~ 200 μm wide slits can be cut on 3 μm i.d. to 500 μm i.d. capillaries by choosing an appropriate thickness of blade. Private communication with Zare proves that drilling holes with CO_2 laser on capillary is not easy for other research groups. The size of the holes drilled by CO_2 laser is not easy to control.

(2) The size of the slits made by the wafer dicing saw are greatly reproducible.

(3) Model 1100 wafer dicing saw demonstrates an incredible processing speed. Model 1100 wafer dicing saw can cut one slit radially or longitudinally on three hundred 52 μm i.d. x 360 μm o.d. capillaries within 20 minutes. In other word, it takes 4 seconds to cut one slit in one capillary. Such a high speed is ideal for mass production.

(4) Model 1100 wafer dicing saw is able to cut the cross-section of 20 μm i.d. ~ 500 μm i.d. capillaries longitudinally with great accuracy.

2.9 Construction of end-column conductivity cell

2.9.1 Fabrication of platinum sensing electrode

15 mm long x 50.8 μm diameter platinum wire was cut radially with a sharp razor blade on a precleaned microscope slide. The end of the platinum wire should not be distorted otherwise it is very difficult to insert it into the internal hole of the 52 μm i.d. x 360 μm o.d. capillary. The end of the Pt wire was examined under microscope after each cutting until a flat cross-section was achieved. Figure 2.12 shows the cross-section of 50.8 μm diameter platinum electrode in detail. It is easy to repeat the same quality. The method to achieve an optical flat cross-section of platinum electrode is described in the section of future work.
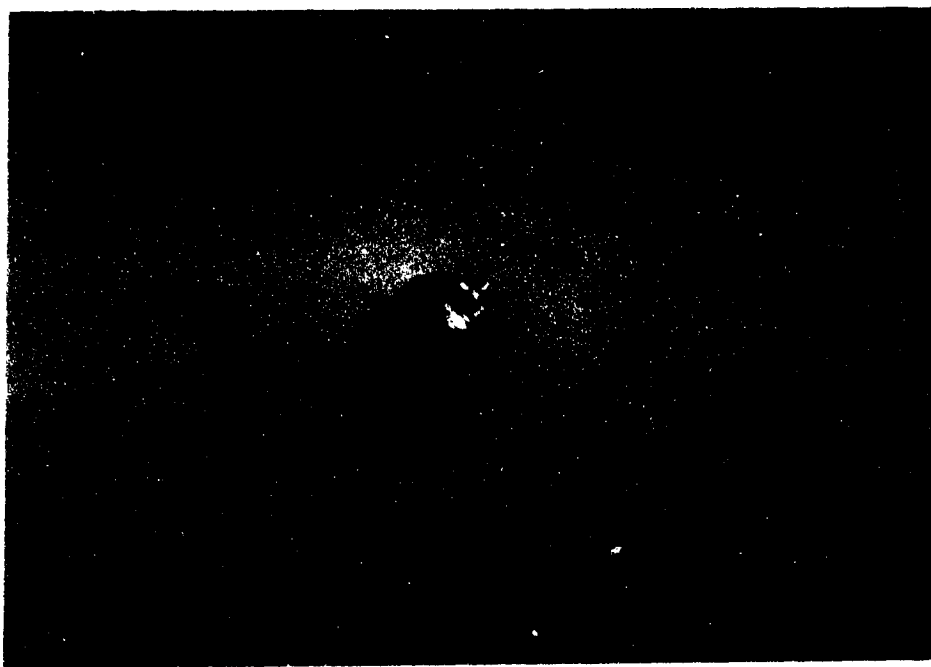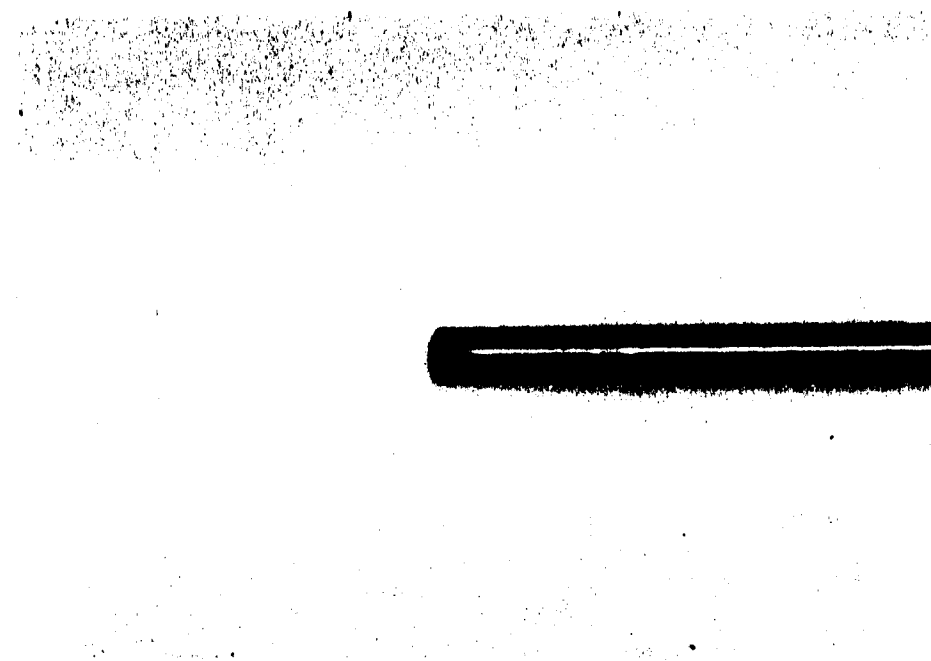
Figure 2.12

50.8 μm diameter platinum wire was cut with a sharp razor blade

2.9.2 Conductivity cell holder

10 cm long sheath was peeled from a 50 cm long coax cable. The core was made into a 1/8" diameter coil around a stainless steel tubing. This coil was then inserted into a 1/8" i.d. x 1/4" o.d. x 2" long Plexiglas tubing (Johnston Industrial Plastics Ltd., Edmonton, Alberta) on which a 1/32" deep V-groove was machined. Pour the mixture of powder and liquid of Dura Lay (Reliance Dental mfg, Co., Worth, Ill, U.S.A.) into the tubing and allow it to cure for two hours.

2.9.3 Insertion of sensing platinum electrode

A 55 μm wide x 164 μm deep slit was cut exactly 10 mm from the end of 40 cm long x 52 μm i.d. x 360 μm o.d. capillary as shown in figure 2.6. A 15 mm long x 50.8 μm diameter platinum wire was manually inserted to the position 2 as shown in figure 2.14 (top) using a sharp-tip forceps (Dumont, Switzerland) under microscope. Figure 2.13 shows the configuration of end-column conductivity cell in capillary zone electrophoresis. In order to present a clear photograph of this delicate and tiny structure the slit and platinum electrode was shot from three directic The capillary without platinum electrode was used for contrast. The platinum wire was then sealed to the capillary outlet with Araldite epoxy. This capillary was then glued to the V-groove in the conductivity cell holder with the mixture of powder and liquid of Dura Lay (Reliance Dental mfg, Co., Worth, Ill, U.S.A.). The mixture becomes solid within an hour. The platinum wire was soldered to the core of the above-mentioned coax cable which connects with the conductivity detector. Aradite epoxy was again applied to seal the end. Figure 2.13 (e) is the cross-sectional view of this end-column conductivity detector.

(a)

(b)

Figure 2.13

Configuration of end-column conductivity cell in capillary zone electrophoresis

(c)

(d)

Figure 2.13 (continued)

Configuration of end-column conductivity cell in capillary zone electrophoresis

Capillary: 40 cm x 52 μm i.d. x 360 μm o.d.; slit: 55 μm wide x 164 μm deep

Platinum electrode: 15 mm long x 50.8 μm diameter.

(e)

52 μm i.d. x 360
μm o.d. capillary

1/32" deep, right
angle V groove

lead
wire

1/8"
dia.

1/4"
dia.
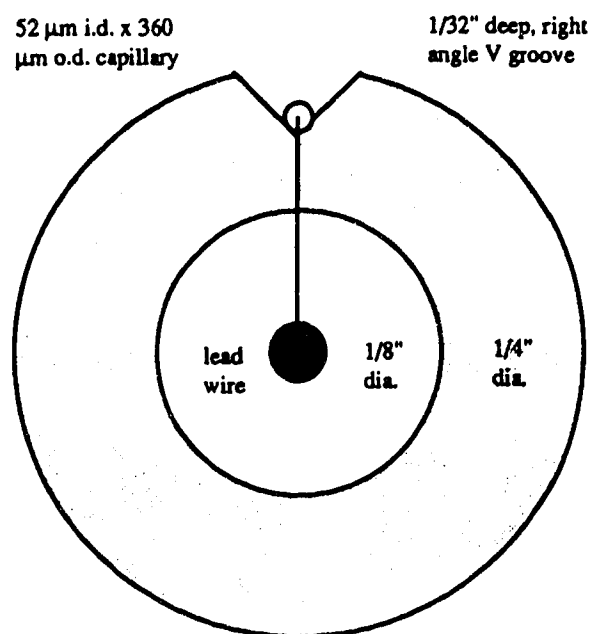
(f)
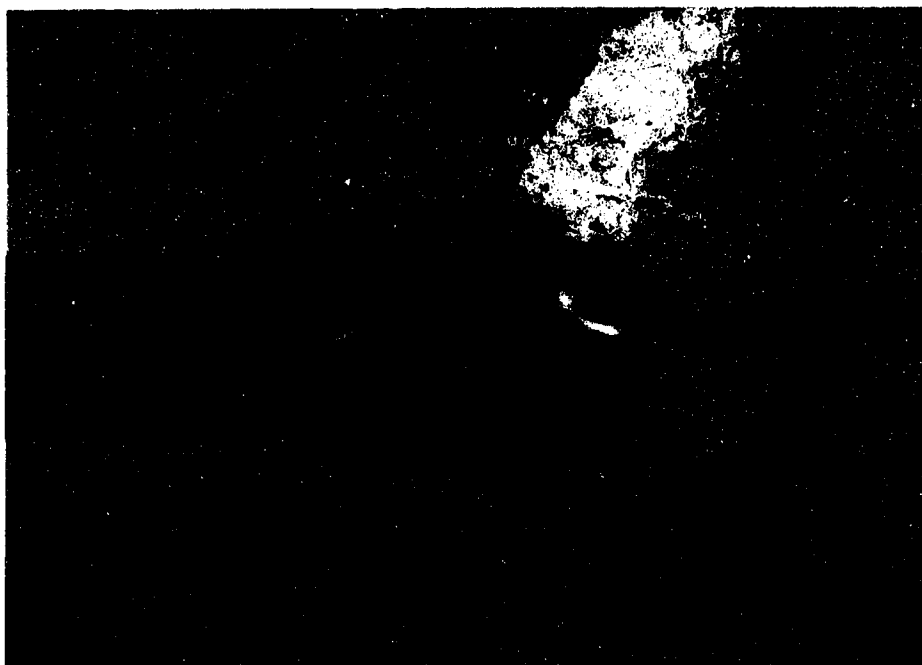
Figure 2.13 (continued)

Configuration of end-column conductivity cell in capillary zone electrophoresis

Capillary: 40 cm x 52 μm i.d. x 360 μm o.d.; slit: 55 μm wide x 164 μm deep

Platinum electrode: 15 mm long x 50.8 μm diameter.

2.6 Electronic circuit for conductivity detection

The electronic circuit of the conductivity detector is shown in Figure 2.15. A function generator (Health Company Benton Harbour, Michigan, USA) supplied a 5 kHz, 0.6 V peak-peak sine wave signal across the platinum sensing electrode inside the capillary and grounding electrode where the conductivity was measured. The signal amplitude was read from Tektronix 2213A, 60 MHz oscilloscope. The applied sine wave signal was ac-coupled through a 0.47 μf capacitor to eliminate the possible electrochemical reaction that might be incurred by any dc bias voltage. The 39.3 kΩ resistor is used to pass the electrophoretic current. The 0.1 μf capacitor passes the high frequency ac signal but rejects low frequency noise. The current through the cell was amplified with two current-to-voltage converters made from LF 356 JFET operational amplifier with a 100 kΩ feedback resistor in parallel with a 5 pf capacitor. The ac output is proportional to the conductivity of the solution between the sensing electrode and the ground electrode. A germanium 1N 617 diode was used to rectify the amplified ac signal. The other 1N 617 diode was used to provide a 0.4 V dc offset to reduce the loss of ac signal. The rectified signal was then conditioned with a summing amplifier constructed from LF 353 after being smoothed with a 0.47 μf capacitor. Eventually, the output was low-pass filtered to remove the high frequency noise.
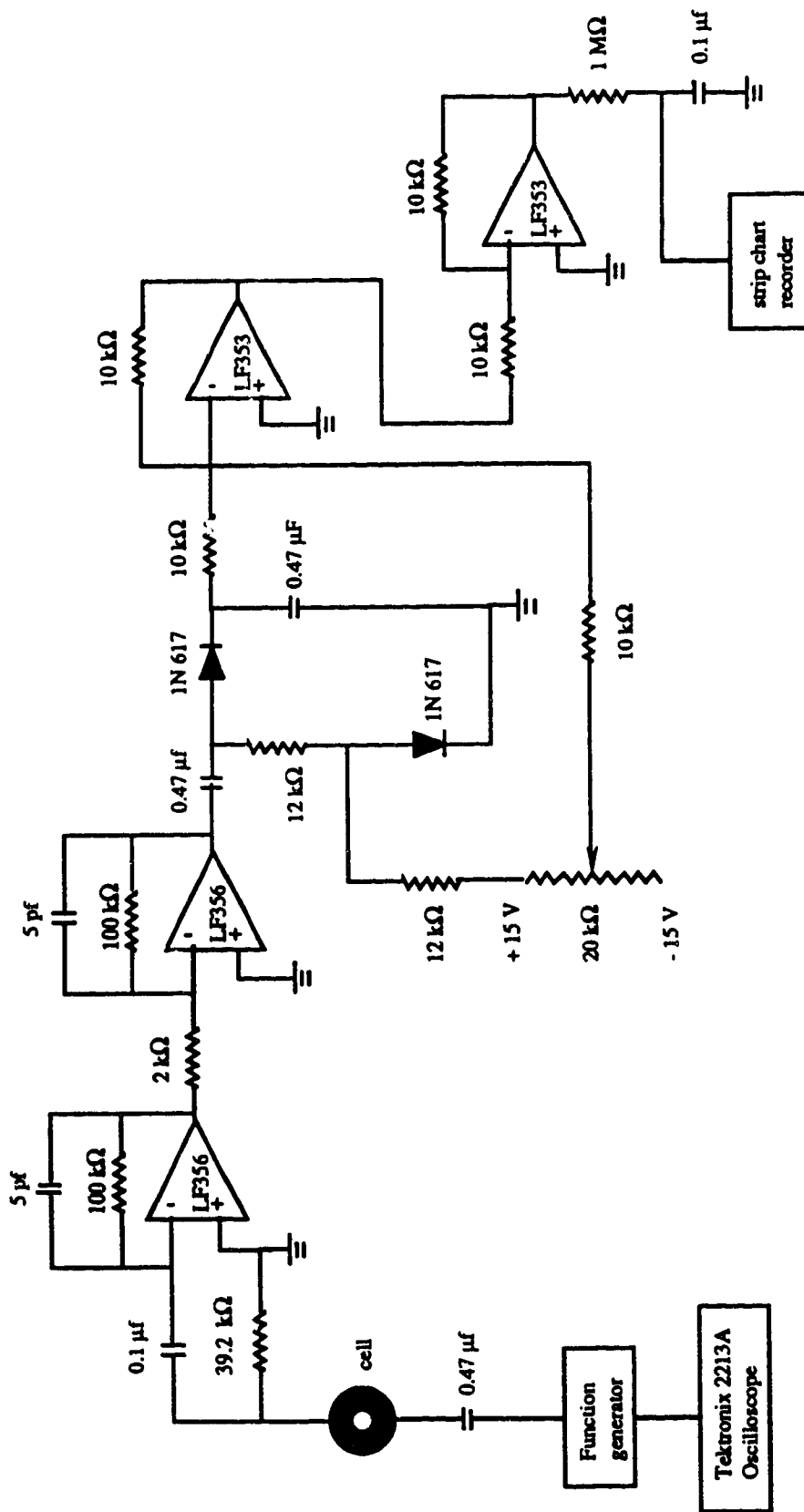
Figure 2.14   Electronic circuit for conductivity detection in capillary zone electrophoresis

CHAPTER III

RESULTS AND DISCUSSION

3.1 Effect of temperature on background conductivity

Temperature has a strong impact on conductivity. The conductivity of an aqueous solution rises about 2 % per degree (50,65). Therefore, it is important to keep the temperature of the conductivity cell constant during electrophoresis. This can be accomplished by thermostating the conductivity cell slightly above ambient temperature.

In the present experiment, the conductivity was measured inside a 25 ml buffer reservoir at room temperature (about 22 °C). The conductivity cell was not thermostated for the purpose of simplicity. The electrophoretic current in this experiment was 2.4 μA under 10 kV applied voltage. The total power generated was 0.024 W, which could change temperature less than 0.3 °C according to Burgi' s work (5). When 10 kV was applied across the capillary, it took 157 seconds for K^+ to migrate through the 40 cm long capillary. The sum of electrophoretic and electroosmotic flow for K^+ was calculated to be 2.548 mm / seconds. The detector holder was immersed 5 cm into the buffer, it was 4 cm from the slit to the surface of the ground buffer. Therefore, the flow of eluent was cooled by the ground buffer for about 16 seconds. This helped to reduce the thermal convection in the vicinity of the sensing platinum electrode when higher power was delivered across the capillary.

3.2 Effect of platinum sensing electrode on the electrophoretic current

Huang and Zare (37) demonstrated that the electrophoretic current fluctuated wildly after 1-2 min and then declined for position 1 and 2 of the platinum sensing electrode in the end-column conductivity detector, as shown in figure 3.1, when high voltage (300 V / cm) was applied. They suspected that gas bubbles accumulating around the sensing electrode caused this undesirable behavior. To investigate whether this was true in our conductivity detector, the electrophoretic current was recorded for 30 minutes under 15 kV / 40 cm (375 V / cm) electric field. The current (3.7 μA) turned out to be constant
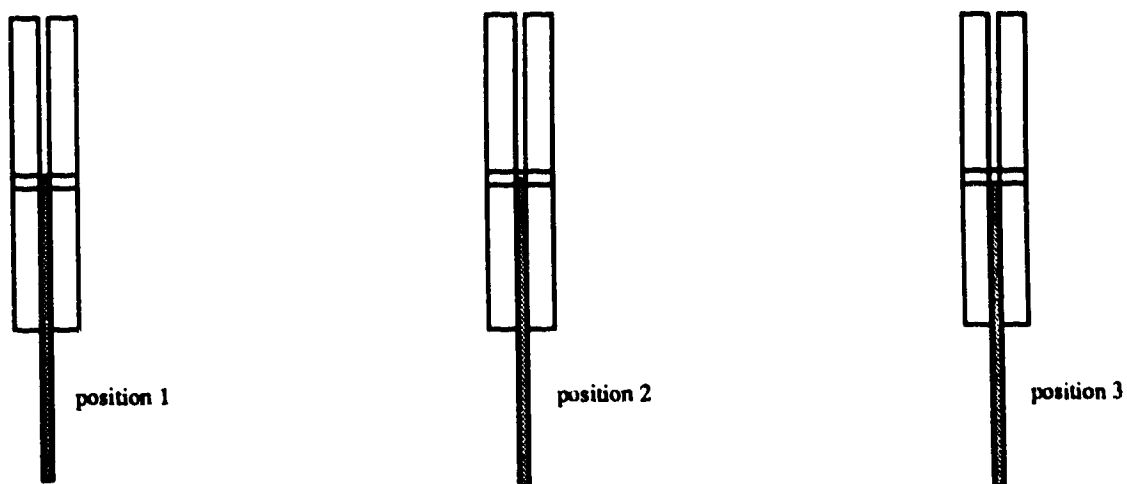
Figure 3.1

Three positions of the 50.8 μm diameter platinum sensing electrodes in CZE

The 164 μm deep x 55 μm wide slit is 10 mm from the end of 52 μm i.d. x 360 μm o.d. capillary. Position 1: top; position 2: middle; position 3: bottom.
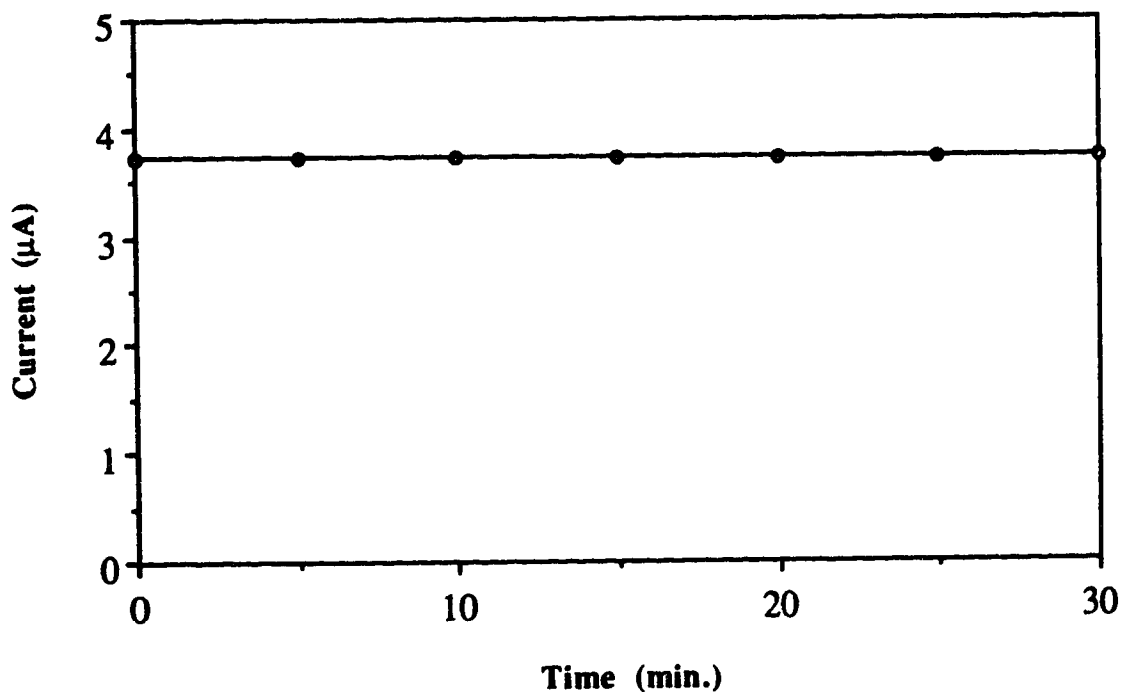
Figure 3.2

Effect of the 50.8 μm dia. platinum sensing electrodes on the current in CZE

Capillary: 40 cm long x 52 μm i.d. x 360 μm o.d.

voltage: 15 kV; current: 3.7 μA; buffer: 20 mM MES / histidine, pH = 6.15

Electrophoretic current (μA)

0   5   10   15   20

Applied voltage (kV)
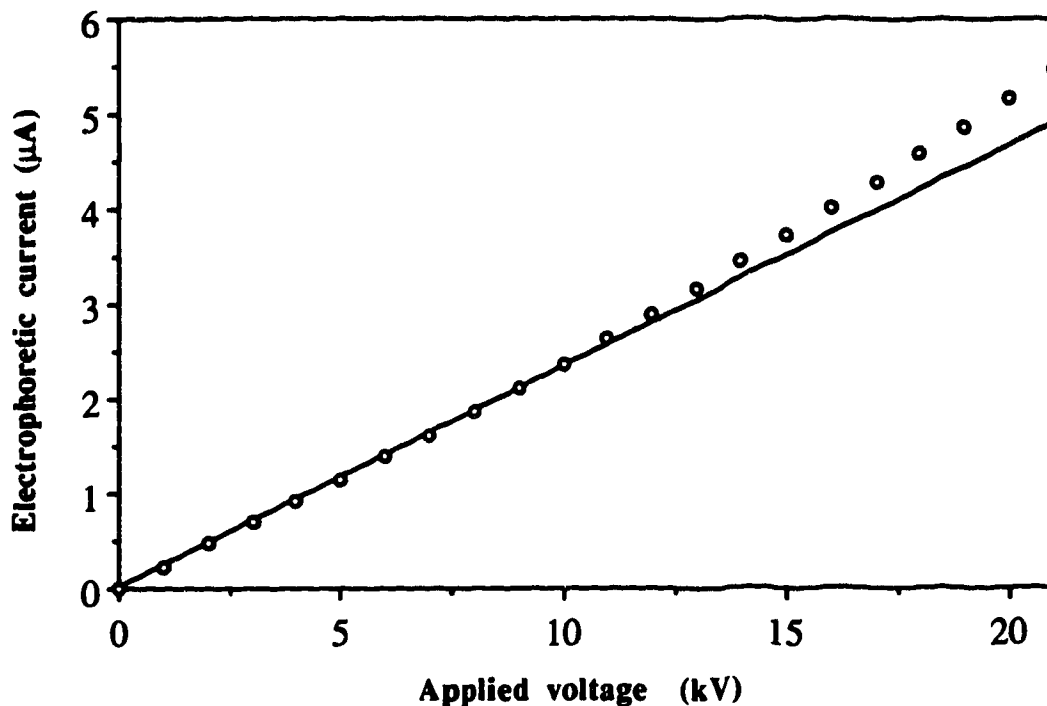
Figure 3.3

The response of the electrophoretic current versus the electrophoretic voltage

Capillary: 40 cm long x 52 μm i.d. x 360 μm o.d.; buffer: 20 mM MES / mM histidine, pH = 6.15.

during the entire electrophoresis as shown in figure 3.2. Therefore, the position 2 of the sensing electrode does not interrupt the electrophoretic current at all. To further study the influence of the sensing electrode, the electrophoretic current was measured under various applied voltages. It was found to be linear with the applied voltage in the range of 0 ~ 12 kV, as shown in figure 3.3. The positive deviation from the linear curve results from the temperature rise induced by the increasing Joule heating. The electrophoretic current increases by 2 % per degree. Figure 3.2 and Figure 3.3 show that position 2 of the sensing electrode does not affect the electrophoretic current. This is different from Huang' s result. This probably results from the different configuration of the conductivity cell. In this conductivity cell, a 164 μm deep x 55 μm wide slit was used rather than a

hole to release the eluent. It is more difficult for gas bubbles to be trapped inside the slit than in a hole. Position 1 conductivity cell was not constructed because the sensing electrode may have blocked the flow of eluent.

3.3 Potential drop between the platinum sensing electrode and ground

A significant advantage of the end-column conductivity detector is the lower potential drop on the platinum sensing electrode. If the sensing electrode in the on-column detector is 1 cm from the capillary outlet when 300 V / cm electric field is applied, it will suffer 300 V which makes the conductivity detection very difficult and dangerous. Therefore, a specially designed electronic circuit for conductivity detection is required (30). However, the potential drop on the sensing electrode in the end-column conductivity detector is only a few volts because the sensing platinum electrode is very close to the ground buffer. A large resistance from the sensing electrode to the bulk buffer means a large potential drop between them. In this conductivity cell, the cross-sectional area of the narrow slit is several times larger than that of the hole drilled by a CO_2 laser, thus the resistance of the buffer inside the narrow slit is predicted to be several times smaller. The potential drop on the sensing electrode was only 1.037 V under 250 V / cm electric field. When 300 V / cm electric field was applied, the potential drop was 1.352 V. This is an apparent improvement compared with the 6.0 V potential drop on the sensing electrode under 300 V / cm electric field reported by Huang (37).

It should be emphasized that the grounding electrode is not a real ground due to the 39.2 kΩ current-sampling resistor. The total resistance from the high voltage end to the grounding electrode is calculated to be 4216 MΩ based on the ratio of voltage to current at 10 kV. In other words, the resistance is 105.4 MΩ / cm, or 1.05 MΩ / 100 μm along the capillary. The total resistance from the sensing platinum electrode inside the 52 μm i.d. x 360 μm i.d. to the real ground is calculated to be 437.2 kΩ. Therefore, the net resistance from the sensing platinum electrode to the grounding electrode is 398 kΩ

which equals the resistance of a 37.9 μm long capillary-filled 20 mM MES / histidine. The semi-circular geometry of the 164 μm deep x 55 μm wide slit reduces the resistance about four times compared with the hole drilled by a CO_2 laser.

3.4 Peak Identification

The identification of the cation peaks in the electropherogram is based on their retention times. The retention time of each cation was measured and summarized in Table 3.1. A 5 x 10^{-5} M cation sample of various cations was electrokinetically injected for 10 seconds at 1 kV. The relative retention time of each cation to lithium is calculated. The absolute mobility of the ions was calculated from the limiting ionic conductance. If the μ^o of the cations is not too close to one another, they should be well separated in the conductivity detection of capillary zone electrophoresis.

Table 3.1   Retention time and relative retention time of Li^+, Na^+, K^+ and Rb^+

Cation	Retention time t_r	t_r / t_r (Li^+)	μ^o (10^{-8} m^2 / s V)
Li^+	240	1.000	4.01
Na^+	203	0.8458	5.19
K^+	155	0.6458	7.62
Rb^+	149	0.6208	8.06

t_r / t_r (Li^+): relative retention time Li^+; μ^o: absolute mobility of ions from (ref. 88). Analyte: 5 x 10^{-5} M LiCl, NaCl, KCl and RbCl; Buffer: 20 mM MES / histidine, pH = 6.15; electrophoretic voltage: 10 kV; injection voltage: 1 kV for 10 second; electrophoretic current: 2.4 μA; capillary: 40 cm long x 52 μm i.d. x 360 μm o.d.; sinewave amplitude: 0.6V; potential drop on sensing electrode: 1.037 V;

Based on the data in Table 3.1, the absolute mobility of 20 mM MES / histidine buffer is calculated to be 2.46 x 10^{-8} m^2 / s V according to equation (3.1):

$$t_{r\,Li}(\mu_{eo}+\mu^O_{Li})\,V_{ep} = t_{r\,Na}(\mu_{eo}+\mu^O_{Na})\,V_{ep} \tag{3.1}$$

where μ^O_{Li} and μ^O_{Na} are the electrophoretic mobility of Li^+ and Na^+ respectively and V_{ep} is the electrophoretic voltage.

3.5 Precision

The peak height precision for 6 x 10^{-5} M Li^+, Na^+ and K^+ was investigated under conditions described in table 3.2. After each run, the high voltage was left on for 5 minutes to purge the capillary. All the electropherograms were run within the same day. The standard deviation and relative standard deviation of peak height and retention time is listed in table 3.2. The ten runs are shown in figure 3.4.

The deviation in peak height results from the variation of the injection volume from run to run. The injection volume was determined by the injection voltage and injection time according to equation (1.9). It is unlikely that the manual setting of injection voltage could introduce apparent variation. Consequently, the deviation in peak height reflects the variation in the injection time. Higher precision could be achieved if a computer was used to control the injection time and voltage.

run 1

run 2

run 3
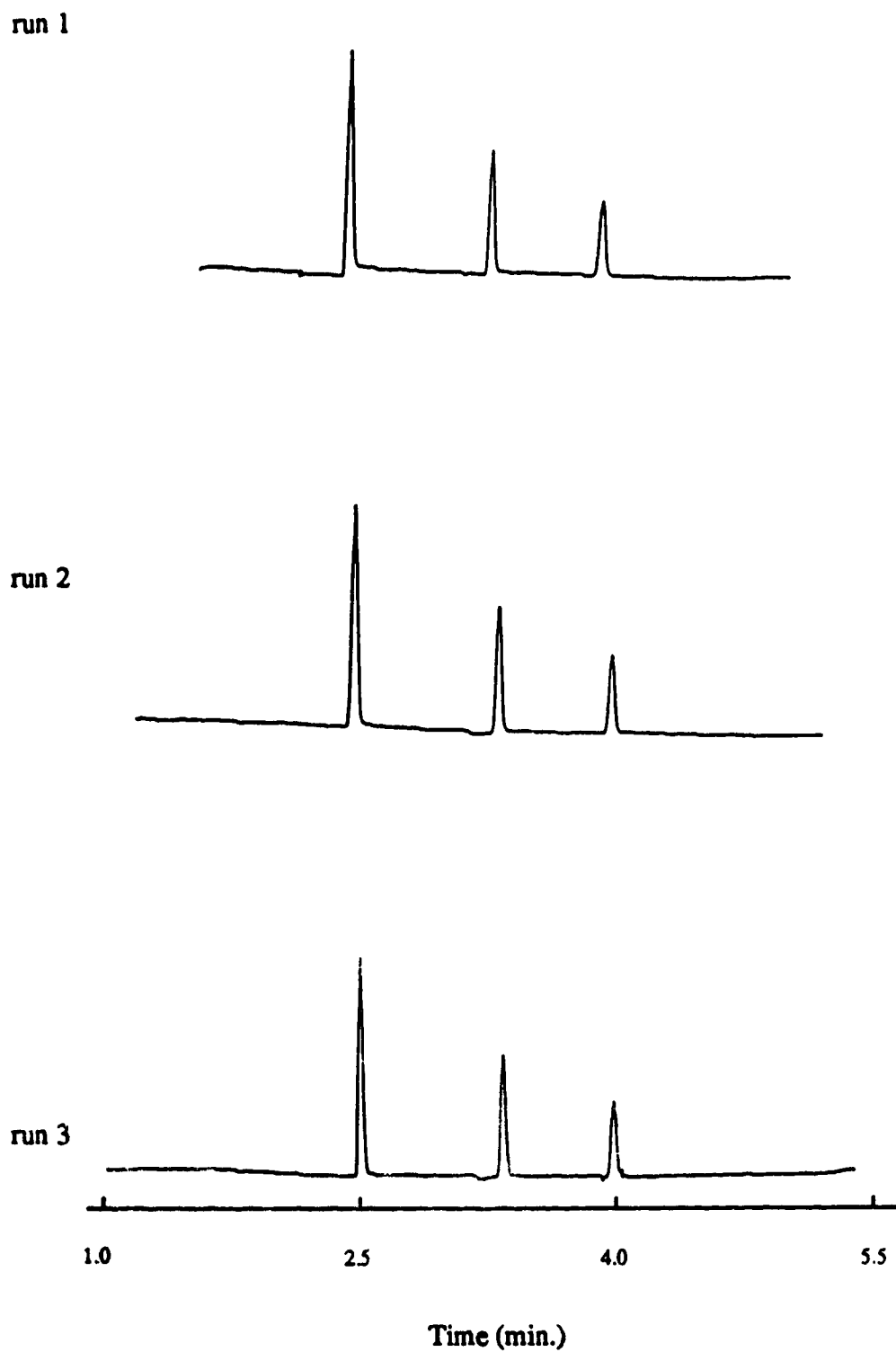
1.0	2.5	4.0	5.5

Time (min.)

Figure 3.4

End-column conductimetric electropherogram for 6×10^{-5} M Li^+, Na^+, K^+

Conditions are the same as described in Table 3.2

run 4
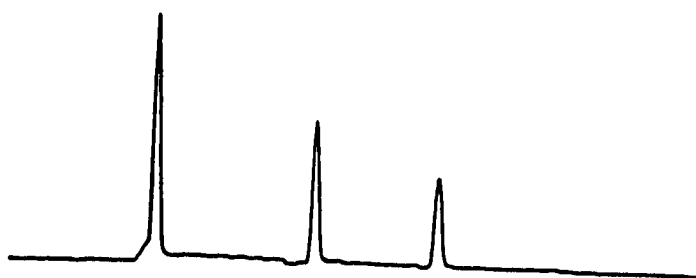
run 5

run 6

1.0   2.5   4.0   5.5

Time (min.)

Figure 3.4 (continued)

End-column conductimetric electropherogram for 6 x 10^{-5} M Li$^+$, Na$^+$, K$^+$

Conditions are the same as described in Table 3.2

run 7

run 8

run9

run 10

Time (min.)

Figure 3.4 (continued)

End-column conductimetric electropherogram for 6 x 10^{-5} M Li$^+$, Na$^+$, K$^+$

Conditions are the same as described in Table 3.2

Table 3.2 Precision of peak height and retention time for 6×10^{-5} M Li^+, Na^+ and K^+

	Peak height (mm)			Retention time (second)		
	Li^+	Na^+	K^+	Li^+	Na^+	K^+
No. 1	11.3	17.7	32.0	241	204	157
No. 2	11.3	17.9	32.2	241	204	157
No. 3	11.0	18.0	31.7	241	203	156
No. 4	11.2	18.1	32.0	239	202	154
No. 5	11.3	18.3	32.4	239	203	156
No. 6	11.5	18.4	31.5	239	203	156
No. 7	11.5	18.3	31.0	239	202	154
No. 8	12.0	18.6	32.0	239	203	155
No. 9	11.2	18.3	32.2	239	202	154
No. 10	11.3	18.7	32.2	238	202	155
Average	11.4	18.2	31.9	240	203	155
STD	0.27	0.31	0.42	1.1	0.79	1.2
RSD	2.4 %	1.7 %	1.3 %	0.46 %	0.39 %	0.77 %

STD: standard deviation; RSD: relative standard deviation.

Buffer: 20 mM MES / histidine, pH = 6.15; electrophoretic voltage: 10 kV;

injection voltage: 1 kV for 10 second; electrophoretic current: 2.4 μA;

capillary: 40 cm long x 52 μm i.d. x 360 μm o.d.; sinewave amplitude: 0.6 V;

potential drop on sensing electrode: 1.037 V;

3.6 Separation efficiency

The separation efficiency was investigated with 5×10^{-5} M LiCl, NaCl, KCl and RbCl. In order to achieve an accurate measurement of peak width, the paper speed of the strip chart recorder was increased to 5 inch / min. However, the real paper speed was measured from the retention time of Rb^+ and Li^+ for each run. A stop watch was used to record the retention of each cation. The injected volume of each cationic component was calculated according to equation (1.9). The total volume of the separation capillary (40 cm long x 52 μm i.d. x 360 μm o.d.) was calculated to be 849 nl. The number of theoretical plates was calculated according to equation (1.5). Figure 3.3 demonstrated that the peaks became more and more asymmetric from Li^+ to Rb^+, which means that the column was overloaded gradually. This was evident by the decreasing number of theoretical plates as shown in table 3.3 for Li^+ to Rb^+. To avoid distortion of the peak shape, the ionic strength of the sample must be much less (1%) than the ionic strength of the separation buffer (93). Otherwise, at higher concentrations, the sample will perturb

Table 3.3   Number of theoretical plates for 5×10^{-5} M Li^+, Na^+, K^+ and Rb^+

	Li^+	Na^+	K^+	Rb^+
Retention time (s)	240	204	157	149
Baseline peak width (s)	2.5	2.2	1.8	2.0
No. of theoretical plates	150000	140000	120000	87000
Injected volume (nl)	0.88	1.04	1.35	1.42

Sample: 5×10^{-5} M Li^+, Na^+, K^+ and Rb^+; Buffer: 20 mM MES / histidine, pH = 6.15; electrophoretic voltage: 10 kV; injection voltage: 0.5 kV for 5 seconds; current: 2.4 μA; sinewave amplitude: 0.6 V; potential drop on sensing electrode: 1.037 V; capillary: 40 cm long x 52 μm i.d. x 360 μm o.d.

Time (min.)
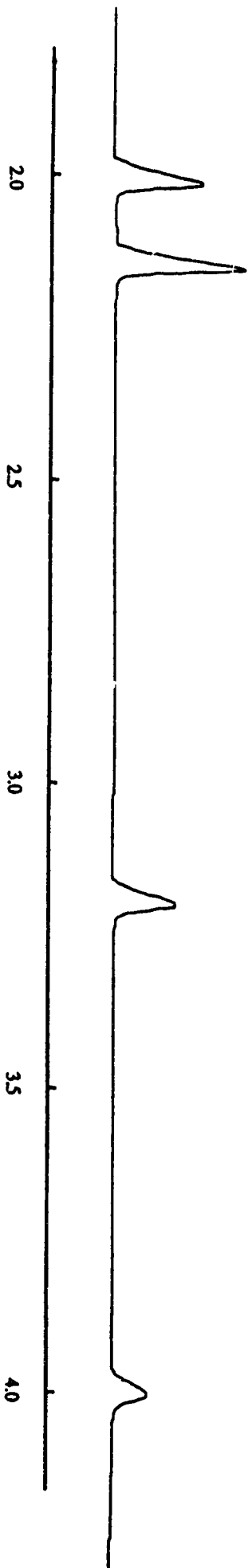
Figure 3.5
End-column conductimetric electropherogram for 5×10^{-5} M Li$^+$, Na$^+$, K$^+$, Rb$^+$ in CZE
Sample: 5×10^{-5} M Li$^+$, Na$^+$, K$^+$ and Rb$^+$; Buffer: 20 mM MES / histidine, pH = 6.15;
electrophoretic voltage: 10 kV; injection voltage: 0.5 kV for 5 seconds; current: 2.4 μA;
capillary: 40 cm long x 52 μm i.d. x 360 μm o.d.; sinewave amplitude: 0.6 V;
potential drop on sensing electrode: 1.037 V;

the local electric field, causing either peak fronting or tailing (54, 55). The number of theoretical plates can be increased by increasing the concentration of the separation buffer.

3.7 Calibration

A calibration curve for Li^+, Na^+ and K^+ was constructed under the conditons described in figure 3.6. Figure 3.7 is a group of electropherograms for 8×10^{-5} M Li^+, Na^+ and K^+.
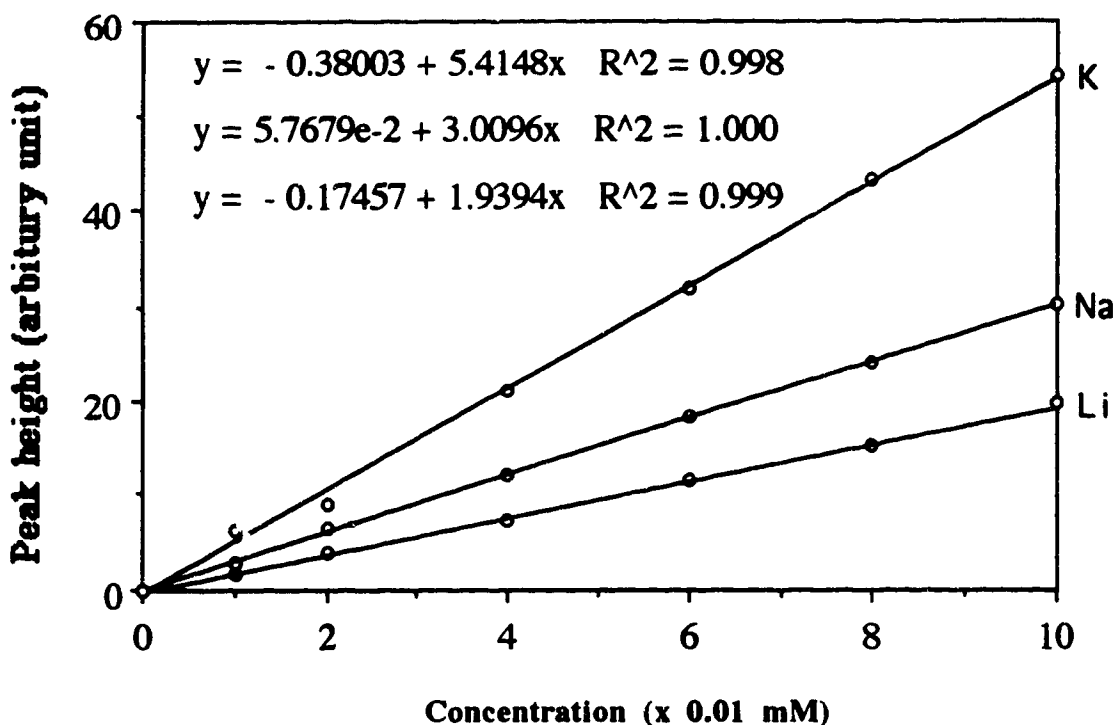
Figure 3.6

Calibration curve for Li^+, Na^+ and K^+ in the end-colum conductivity detection in CZE

Buffer: 20 mM MES and 20 mM Histidine, pH = 6.15; electrophoretic voltage: 10 kV; injection voltage: 1 kV for 10 s; current: 2.4 μA; sinewave amplitude: 0.6 V; potential drop on platinum sensing electrode: 1.037 V

capillary: 40 cm long x 52 μm i.d. x 360 μm o.d.;
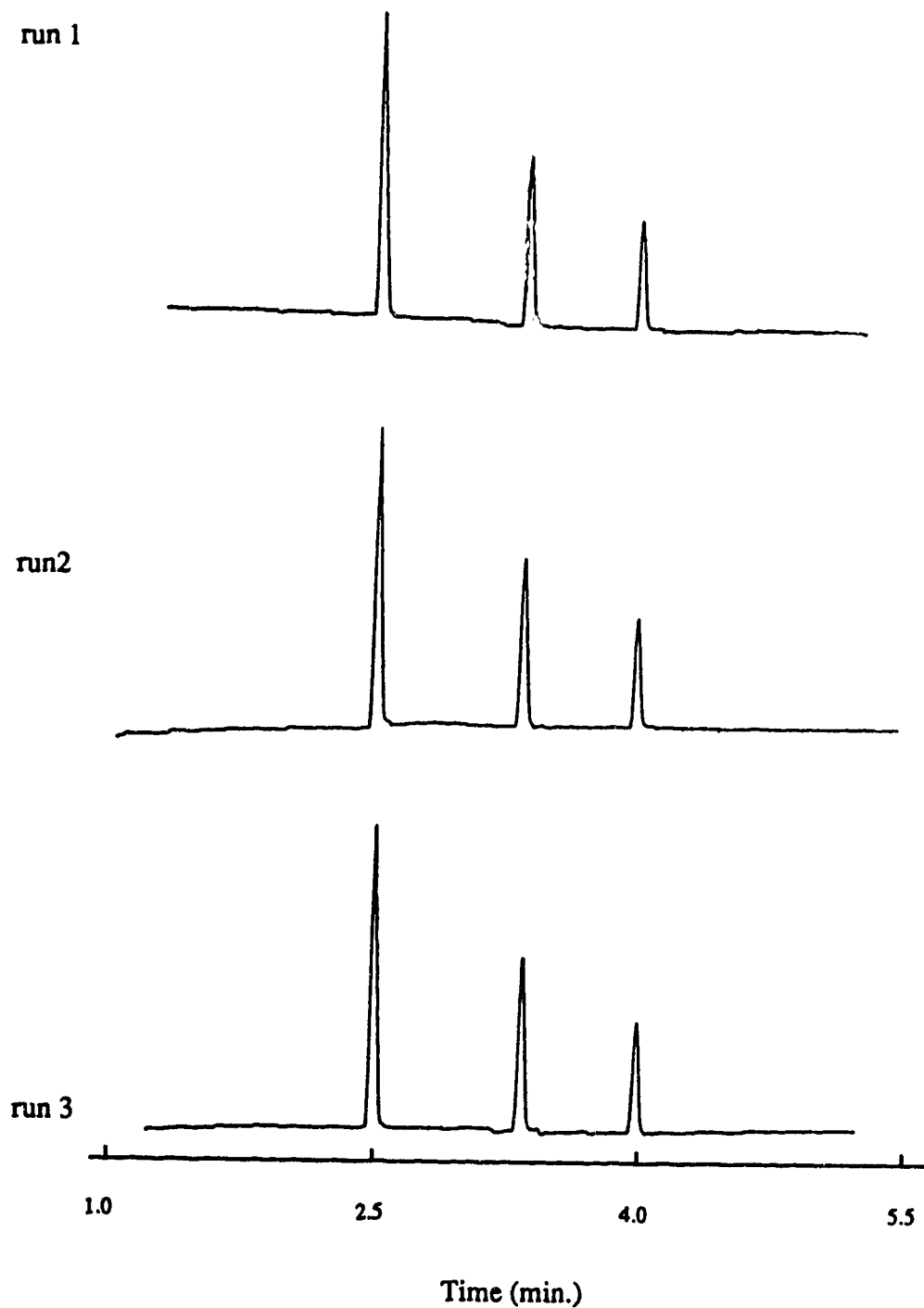
Figure 3.7

End-column conductimetric electropherograms for 8×10^{-5} M Li^+, Na^+, K^+ in CZE.

Sample: 8×10^{-5} M Li^+, Na^+, K^+; Buffer: 20 mM MES / histidine, pH = 6.15;

electrophoretic voltage: 10 kV; injection voltage: 1 kV for 10 seconds; current: 2.4 μA;

potential drop on sensing electrode: 1.037 V; sinewave amplitude: 0.6 V;

capillary: 40 cm long x 52 μm i.d. x 360 μm o.d.

3.8 Evaluation of the limit of detection

Figure 3.8 shows the noise fluctuation during one minute of electrophoresis when 10 kV high voltage was applied across the capillary. The sensitivity of the strip chart recorder was set to 0.001V. The amplitude of noise was estimated to be 10 mm on the 0.001 V sensitivity scale or 0.1 mm on a 0.1 V sensitivity scale on the strip chart recorder. The amplitude of the noise level is mainly related to the fluctuation of the applied voltage. Sometimes this fluctuation was found to be serious during the daytime, therefore all the experiments were done in the night time. Detection limit was calculated using Knoll' s method (44) on 20 times peak width at one-half peak height. The results were listed in table 3.4.

Table 3.4

Estimation of the limit of detection in the end-column conductivity detector in CZE

	Injection volume (nl)	LOD (concentration: 10^{-7} M)
Li^+	3.52	7.38
Na^+	4.16	4.75
K^+	5.40	2.64
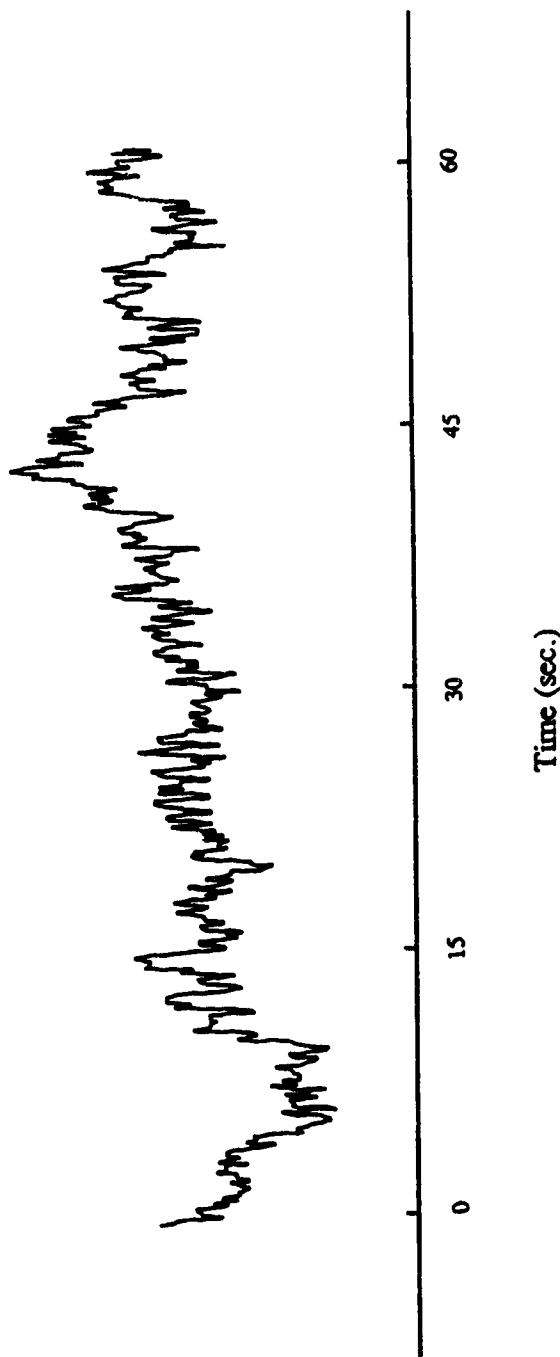
Figure 3.8

Noise test for the end-column conductivity detection in capillary zone electrophoresis

Applied high voltage: 10 kV; potential drop on platinum sensing electrode: 1.037 V

electrophoretic current: 2.4 µA; capillary: 40 cm long x 52 µm i.d. x 360 µm o.d.;

buffer: 20 mM MES / histidine, pH = 6.15.

3.9 Mathsmatic model for the resistance of a non-uniform solution

The conductivity was measured between the platinum sensing electrode, located at the middle of the 164 μm deep x 55 μm wide slit and the ground electrode. Therefore, the conductance of the buffer inside the ground reservoir must be taken into account, as regard to whether it affects the conductivity signal measured. In fact, it was proved experimentally that it played no role on the conductivity signal (37). To understand why the conductivity signal is not affected by the bulk buffer in the ground reservoir, a mathsmatic model based on integration is established to predict the resistance of the buffer in the 164 μm deep x 55 μm wide slit and the bulk buffer in the ground reservoir.

3.9.1 Resistance of the buffer inside the narrow slit

According to Ohm' s Law, the resistance for an uniform electrolytic solution can be given by

$$R = \rho \frac{L}{A} \tag{3.2}$$

where R is the resistance of the electrolytic solution, ρ is the resistivity of the electrolytic solution. L is the distance between the two electrodes. A is the surface area of the electrodes. This equation is not valid for an electrolytic solution in a non uniform container. The buffer in the 164 μm deep x 55 μm wide slit represents this situation. In order to solve the problem, it is assumed the buffer in the slit is connected seriesly via n layers of semi-circular buffer as shown in figure 3.8. Since the platinum sensing electrode is only inserted into the middle of the slit, thus the width of the layer, w_i, is given by

$$w_i = \frac{w_s\, r_i}{2\, r_c} + \frac{w_s}{2} = \frac{w_s\, (\, r_i + r_c\,)}{2\, r_c} \tag{3.3}$$
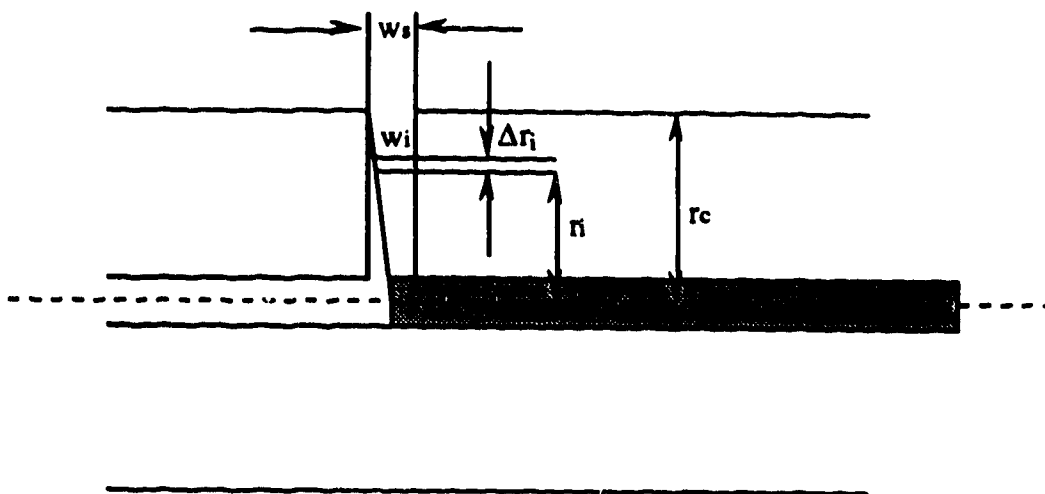
Figure 3.9

Schematic representation of the buffer inside the 164 μm deep x 55 μm wide slit on the 52 μm i.d. x 360 μm o.d. fused silica capillary (not draw on scale)

sensing electrode (50.8 μm)
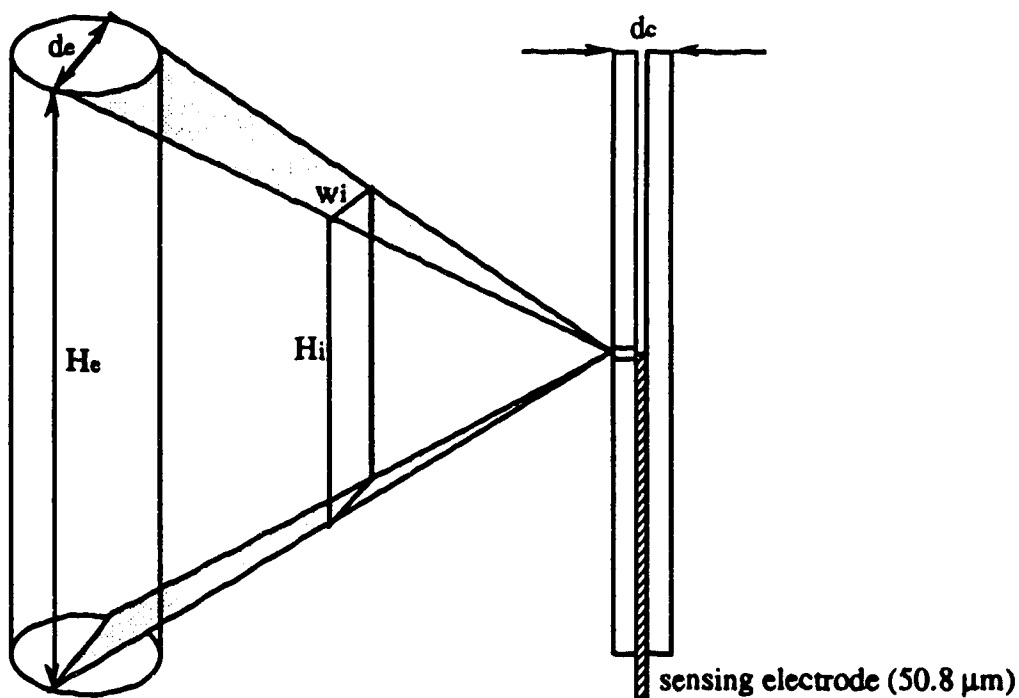
Figure 3.10

Schematic representation of the bulk buffer in the ground reservoir (not draw on scale)

Capillary: 40 cm x 52 μm i.d. x 360 μm o.d.; ground electrode: 5 cm long x 0.8 mm dia.

where r_i is the radius of the layer; Δr is the thickness of the layer; w_s is the width of the slit, 55 μm; r_c is the radius of the capillary. The surface area of a random layer of buffer is given by the function

$$A_i = \pi\, r_i\, w_i = \frac{\pi\, r_i \setminus ',\, (r_i + r_c)}{2\, r_c} \tag{3.4}$$

The resistance is given by the formula

$$R_i = \rho\, \frac{\Delta r_i}{A_i} = \frac{2\, \rho\, r_c\, \Delta r_i}{\pi\, r_i\, w_s\, (r_i + r_c)} \tag{3.5}$$

The overall resistance is given by the sum of resistance from each layer of buffer in the slit

$$R = \sum_{i=1}^{n} \rho\, \frac{\Delta r_i}{A_i} = \sum_{i=1}^{n} \frac{2\, \rho\, r_c\, \Delta r_i}{\pi\, r_i\, w_s\, (r_i + r_c)} \tag{3.6}$$

as $n \to \infty$, R becomes a problem of definite integral from the surface of the platinum sensing electrode to the outer surface of the capillary, thus we have

$$R = \int_{r_p}^{r_c} \frac{2\, \rho\, r_c}{\pi\, r\, w_s\, (r + r_c)}\, dr \tag{3.7}$$

where r_p is the radius of the platinum sensing electrode, 25.4 μm. Solving this definite integral, we have

$$R = \frac{2\, \rho\, r_c}{\pi\, w_s} \int_{r_p}^{r_c} \frac{1}{r\, (r + r_c)}\, dr$$

$$= \frac{2\,\rho\,r_c}{\pi\,w_s\,r_c} \int_{r_p}^{r_c} (\frac{1}{r} - \frac{1}{r+r_c})\, dr$$

$$= \frac{2\,\rho}{\pi\,w_s} [\, \ln r - \ln(r+r_c)\,]_{r_p}^{r_c}$$

$$= \frac{2\,\rho}{55\,\pi} [\, \ln \frac{180}{25.4} - \ln \frac{180+360}{25.4+360}\,]$$

$$= 1.9 \times 10^{-2}\ \mu m^{-1}\,\rho$$

3.9.2 Resistance of the bulk buffer in the ground reservoir

Compared with the height of the ground electrode immersed in the buffer, the width of the slit can be assumed as a infinitely small point. The length of the slit (360 µm) should not be ingored. The ground buffer is assumed to be connected seriesly via layers of rectangular buffer from the slit to the ground electrode, as shown in figure 3.9. The height of a random layer of buffer is given by the function

$$H_i = \frac{L_i\,H_e}{L_{es}} \tag{3.8}$$

where L_{es} is the distance from the slit to the ground electrode, 2 mm. H_e is the height of the ground electrode immersed in the ground buffer, 50 mm. The width of a random layer of buffer is given by the function

$$W_i = \frac{(d_e - d_c)\,L_i}{L_{es}} + d_c = \frac{(d_e - d_c)\,L_i + L_{es}\,d_c}{L_{es}} \tag{3.9}$$

d_e is the diameter of the ground platinum electrode, 0.8 mm. d_c is the diameter of the capillary, 0.360 mm.

$$A_i = H_i \times W_i = \frac{L_i H_e [(d_e - d_c) L_i + L_{es} d_c]}{L_{es}^2} \qquad (3.10)$$

The resistance of a random layer of buffer is given by the function

$$R_i = \frac{\rho \, \Delta L_i}{A_i} = \frac{L_{es}^2 \, \rho \, \Delta L_i}{L_i H_e [(d_e - d_c) L_i + L_{es} d_c]} \qquad (3.11)$$

Following the method in 3.6.1, the total resistance from the slit to the ground electrode is given by a definite integral

$$R = \int_{l}^{L_{es}} \frac{\rho}{A} \, dL \qquad (3.12)$$

$$= \int_{l_e}^{L_{es}} \frac{L_{es}^2 \, \rho}{L \, H_e [(d_e - d_c) L + L_{es} d_c]} \, dL$$

$$= \frac{L_{es}^2 \, \rho}{H_e (d_e - d_c)} \int_{l_e}^{L_{es}} \frac{1}{L \, [\, L + \frac{L_{es} d_c}{(d_e - d_c)} \,]} \, dL$$

$$= \frac{L_{es}^2 \, \rho}{H_e (d_e - d_c)} \frac{(d_e - d_c)}{L_{es} d_c} \int_{l_e}^{L_{es}} (\frac{1}{L} - \frac{1}{L + \frac{L_{es} d_c}{(d_e - d_c)}}) \, dL$$

$$= \frac{L_{es} \, \rho}{H_e d_c} [\ln L - \ln (L + \frac{L_{es} d_c}{d_e - d_c})]_{l_e}^{L_{es}}$$

$$= \frac{L_{es} \, \rho}{H_e d_c} [\ln L - \ln [(d_e - d_c) L + L_{es} d_c] + \ln (d_e - d_c)]_{l_e}^{L_{es}}$$

$$= \frac{2\rho}{50 \times 0.360} \left(\ln \frac{2}{0.180} - \ln \frac{(0.8 - 0.360) \times 2 + 2 \times 0.360}{(0.8 - 0.360) \times 0.180 + 2 \times 0.360} \right)$$

$$= 0.19 \, \text{mm}^{-1} \, \rho$$

$$= 1.9 \times 10^{-4} \, \mu\text{m}^{-1} \rho$$

From the results calculated, the resistance of the buffer in the slit is about 100 times that of the bulk buffer in the ground reservoir. Therefore, the buffer in the slit dominates the resistance. The volume of the ground buffer (25 ml) is about 30000 times the volume of the capillary (849 nl). Thus, the eluted sample zone can not change the conductance of the bulk buffer. These explain why the bulk buffer in the ground electrode plays no role on the conductivity signal in our detector from theoretical point of view.

CHAPTER IV

CONCLUSIONS AND FUTURE WORK

Conclusions

In this thesis, a wafer dicing saw was found to be an ideal tool for the radial and longitudinal dicing of small internal diameter fused-silica capillaries. It provides not only an excellent dicing accuracy but also a high processing efficiency for mass production. No additional equipment was required. An easy technique for making two holes with controllable size across the capillary was also demonstrated based on the longitudinal dicing of the capillary. This was the simplest but state of the art non-laser technique to make holes on fused-silica capillary tubing.

The radial dicing of a 52 μm i.d. x 360 μm o.d. capillary was applied for the construction of an end-column conductivity detector in capillary zone electrophoresis. The end-column conductivity detector eliminated the detection problems associated with high voltage drop along the capillary. The major priority of the end-column detection was its simple design and easy construction with the use of wafer dicing saw. The insertion of a 50.8 μm diameter platinum sensing electrode into the 52 μm i.d. fused-silica capillary greatly reduced the chance of air bubbles being trapped between the platinum sensing electrode and the wall of the capillary, thus providing the detector with improved stability and reduced baseline drift.

The concentration limit of detection reached 7.4 x 10^{-7} M for Li^+, 4.8 x 10^{-7} M for Na^+, 2.6 x 10^{-7} M for K^+. This detection limit is comparable to literature values (30, 36, 37). The total cost of the material for the construction of the conductivity cell was less than \$20, which is much cheaper than the conductivity cell widely used in ion chromayography. The application of end-column conductivity detection can be extended to the analysis of inorganic and organic ions. A commercial conductivity detector in capillary zone electrophoresis based on the use of the wafer dicing saw is predicted to become available in the near future.

Future Work

Micro " T " and " Cross "

The wafer dicing saw has shown a tremendous advantages in the area of micro machining. It can be used to make a micro " T " and " Cross " for micro mixing of reagents. For example, a controllable depth of narrow slit can be cut on the centre of the cross-section of 75 μm i.d. x 363 μm o.d. capillary. If we cut a 60 μm deep x 120 μm wide slit on the centre of an array of 75 μm i.d. x 363 μm o.d. capillaries, then we can put two 50 μm x 144 μm o.d. capillaries into the slit, under a microscope. The second 75 μm i.d. x 363 μm o.d. capillary with a 60 μm deep x 120 μm wide slit on the cross-section is aligned and pushed against the 50 μm x 144 μm o.d. capillary. By heating the joint of these four capillaries to 1300 °C, a " Cross " can be melted with good quality. A " T " can be achieved by sealing one of the 50 μm x 144 μm o.d. capillaries or the 75 μm i.d. x 363 μm o.d. capillary.

Fabrication of a sensing electrode

A optically flat cross-section of micro sensing platinum electrode can be polished following the procedures below:

(1) Place dozens of 15 mm long Pt wires side by side inside a mold and glue them together with epoxy.

(2) After the epoxy is cured, grind and polish the platinum wire. The surface is cleaned. If the cross-section of platinum wire is smooth when viewed under a microscope, dissolve the epoxy with organic solvent.

Electronic circuit for conductivity detection

Currently one of the major sources of noise is from the electronic circuit for conductivity detection. A commercially available conductivity detector in ion chromatography may be borrowed for the conductivity detection in capillary zone electrophoresis.

References

1. Ackermans, M. T.; Everaerts, F.M.; Beckers, J. L. *J. of Chromatogr.* 1991, **549**, 345-355.

2. Adamson, A. W. *Physical Chemistry of Surfaces*, second edition, Interscience, New York, Chap. 4, 1967.

3. Altria, K. D.; Simpson, C. F.; Bharij, A.; Theobald, A. E. paper presented at the 1988 Pittsburgh Conference and Exposition, abstract no. **642**, New Orleans, Feburary 1988. See also V. Berry, *LC / GC*, 1988, 6, 484.

4. Balchunas, A. T.; Sepaniak, M. J. *Anal. Chem.* 1988, **60**, 617.

5. Burgi, Dean S.; Salomon, Karen; Chien, Ring-Ling. *J. Liquid C   /natogr.iphy,* 1991, **14(5)**, 847-867.

6. Burton, D. E.; Sepaniak, M. J.; Maskarinec, M. *J. Chromatogr. Sci.* 1986, **24**, 347.

7. Campos, Cora C.; Simpson, C. F. *Journal of Chromatographic Science,* 1992, **30**, 53-58.

8. Carchon, H. and Eggermont, E. *American Laboratory,* 1992, Jan. 67.

9. Chen, D. Y.; Swerdlow, H. S.; Harke, H. R.; Zhang, J. Z.; Dovichi, N. J. *J. of Chromatogr.* 1991, **559**, 237-246.

10. Chen, D. Y.; Harke, H. R.; Rocheleau, M. J.; Zhang, J. Z.; Dovichi, N. J. Capillary Electrophoresis, Abstract **14**, AN-B2, *75 th Canadian Chemical Conference and Exhibition,* 1992, May 31 - June 4.

11. Chen, M.; Cassidy, R. M. *J. Chromatogr.* 1992, **602**, 227-234.

12. Cheng, Y. F.; Dovichi, N. J., *Science, 1989,* **242**, 562.

13. Christensen, P.; Yeung, E. *Anal. Chem.* 1989, **61**, 1344.

14. Dadoo, Rejeev; Colon, Luis A.; Zare, R. N. *Journal of High Resolution Chromatography,* 1992, **15**, 133.

15. Deml, M.; Foret, F; Bocek, P. *J. Chromatogr*. 1985, **320**, 159.

16. Dovichi, N. J.; Cheng, Y. F. *Am. Biotechnol. Lab*. 1989, **7** (2), 10, 12, 14.

17. Everaerts, F. M.; Beckers, J. L.; Verheggen, Th. P. E. M. *Isotachophoresis: Theory, Instrumentation, and Applications* (Elsenier, Amsterdam 1976).

18. Ewing, A. G.; Wallingford, R. A.; Olefirowicz, T. M. *Anal. Chem*. 1989, **61**, 292A.

19. Foret, F.; Deml, M.; Kahle, V.; Bocek, P. *Electrophoresis*, 1986, **7**, 430.

20. Fujiwara, S.; Honda, S. *Anal. Chem*. 1987, **59**, 487.

21. Garcia, Frederick; Henion, Jack D. *Anal. Chem*. 1992, **64**, 985-990.

22. Gassmann, E.; Kuc, J.; Zare, R. *Science*, 1985, **230**, 813.

23. Giddings, G. C. *Sep. Sci*. 1989, **4**, 181.

24. Gordon, M. J.; Huang, X. *Science*, 1988, **242**, 224.

25. Grocott, S. C.; Jefferies, L. P.; Bowser, T; Carnevale, J.; Jackson, P. E. J. *Chromatogr*. 1992, **602**, 257 - 264.

26. Guthrie, E.; Jorgenson, J.; Dluzneski, P. *J. Chromatogr*. 1984, **22**, 171.

27. Hargadon, Kelly A.; McCord, Bruce R. *J. of Chromatography*, 1992, **602**, 241 - 247.

28. Higashijima, Toshiyuki; Fuchigami, Tetsuhiro; Imasaka, Totaro; Ishibashi, Nobuhiko, *Anal. Chem*. '92, **64**, 711-714.

29. Hjerten, S. *Chromatogr. Rev*, 1967, **9**, 122-219.

30. Huang, X.; Pang, Teng-Ke J.; Gordon, Manuel J.; Zare, Richard N. *Anal. Chem*. 1987, **59**, 2747.

31. Huang, X.; Luckey, John A.; Gordon, Manuel J; Zare, Richard N. *Anal. Chem*. 1989, **61**, 766.

32. Huang, X.; Gordon, M. J.; Zare, R. N. *Anal. Chem*. 1988, **60**, 375.

33. Huang, X.; Zare, Richard N. *Anal. Chem*. 1990, **62**, 443.

34. Huang, X.; Gordon, M.J.; Zare, R. N. *J. Chromatogr*. 1988, **425**, 385.

35. Huang, X., Gordon, M. J., and Zare, R. N., *J. Chromatogr*. 1989, **480**, 285.

36. Huang, X.; Zare, R.N. *Anal. Chem*. 1991, **63**, 189-192.

37. Huang, X.; Zare, R.N. *Anal. Chem*. 1991, **63**, 2193-2196.

38. Jorgenson, J. W.; Lukacs, K. D. *Anal. Chem*. 1981, **53**, 1298.

39. Jorgenson, J. W.; Lukacs, K. D. *Clin. Chem*. 1981, **27**,1551.

40. Jorgenson, J. W.; Luckcs, K. D. *J. Chromatogr*. 1991, **218**, 209.

41. Jorgenson, J. W. *Anal. Chem*. 1986, **58**, 743A.

42. Jorgenson, J. W.; Lukacs, K. D. *Science*, 1983, **222**, 266.

43. Knecht, Laurance A.; Guthrie, Edward J.; Jorgensen, James. W. *Anal. Chem*. 1984, **56**, 479-482.

44. Knoll, Joseph E., *J. Liquid Chromatography*, 1985, **23**, 422-425.

45. Knox, J. H.; Cormack, K. A. *Journal of Liquid Chromatography*, 1989, **12(13)**, 2435-2470.

46. Koberda, Michael; Konkowski, Mary; Youngberg, Paula; Jones, William R.; Weston, Andrea, *J. Chromatogr*. 1992, **602**, 235-240.

47. Kuhr, W. G.: *Anal. Chem*. 1990, **62**, 403R-414R.

48. Loo, J. A.; Udseth, H. R.; Sr h, R. D. *Anal. Biochem*. 1989, **179** (2), 404.

49. Loo, J. A.; Jones, H. K.; Udseth, H. R.; Smith, R. D. *J. Microcolumn Sep*. 1989, **1**, 223.

50. Loveland, J. W. Conductometry and Oscillometry, in " *Treatise on analytical chemistry* " (Kolthoff, I. M. etal., Ed.) Part I Vol. 4, (1963). John Wiley & Sons.

51. Lukacs, K. D.; Jorgenson, J. W.; *J. High Res. Chromatogr. Chromatogr. Commun*. 1985, **8**, 407.

52. Manz, A.; Simon, W. *J. Chromatographic Science*, 1983, **21**, 326.

53. McCabe, J. *Canandian Chemical News*, 1991, Feb., 16.

54. Mikkers, F. E. P.; Everaerts, F. M.; Verheggan, Th. P. E. M. *J. Chromatogr.* 1979, **169**, 11.

55. Mikkers, F. E. P.; Everaerts, F. M.; Verheggen, Th. P. E. M. *J. Chromatogr.* 1979, **169**, 1.

56. Nickerson, B.; Jorgenson, J. W. *J. High ᴀes. Chromatogr. Chromatogr.Commun.* 1988, **11**, 533.

57. Olechno. J. D.; Tsc. J. M. Y.; Thayer, J. *American Laboratorv* '991, Jan. 59.

58. Olivares, J. A.; Nguyen, N. T.; Y.nker, C. R.; Smith, R. D. *Anal. Chem.* 1987, **59**, 1230.

59. Pentoney, S.; Zare, R.; Quint, J. *Anal. Chem.* 1989, **61**, 1642.

60. Pentoney, S.; Zare, R.; Quint, J. *J. Chromatogr.* 1989, **480**, 259.

61. Romano, Joseph P.; Krol, Jim, *J. of Chromatogr.* 1992, **602**, 205 - 211.

62. Roach, M.; Gozel, P.; Zare, R. *J. Chromatogr.* 1988, **426**, 129.

63. Rose, D. J.; Jorgenson, J. W. *Anal. Chem.* 1988, **60**, 642.

64. Salomon, Delmar R. *J. Chromatogr.* 1992, **602**, 219-225.

65. Shedlovsky, T.; Shedlovsky, L. Conductometry, in *Techniques of Chemistry*, Vol. 1, Physical Methods of Chemistry, Part II A, Electrochemical Methods, Weissberger, A. and Rossiter, B. W., Eds., Johnson Wiley & Sons, New York, (1971)

66. Small, H.; Stevens, T. C.; Bauman, W. C. *Anal. Chem.* 1975, **47**, 1801-1809.

67. Smith, R. A.; Olivares, J. A.; Nguyen, N. T.; Udseth, H. R. *Anal. Chem.* 1988, **60**, 436

68. Smith, R. D.; Barinaga, Charles J., Udseth, H. R. *Anal. Chem.* 1988, **60**, 1948-1952.

69. Smith, R. D.; Udseth, H. R.; Loo, J. A.; Wright, B. W.; Ross, G. A. *Tanlanta* 1989, **36** (1-2), 161.

70. Smith, R. D.; Loo, J.; Barinaga, C.; Edmonds, C.; Udseth, H. R. *J. Chromatogr.* 1989, **480**, 211.

71. Stock, John. T. *Anal. Chem.* 1984, **56**, 561-570.

72. Swaile, D.; Burton, D.; Balchunas, A.; Sepaniak, M. *J. Chromatogr. Sci.* 1988, **26**, 406.

73. Sweedler, J. V.; Shear, J. B.; Fishman, H. A.; Zare, R. N.; Scheller, R. N. *Anal. Chem.* 1991, **63**, 496.

74. Tarter, James. *Chromatographic Science Series Vol. 37, Ion Chromatography*, Marcel Dekker, Inc (1987).

75. Terube, Shigeru; Otsuka, koji; Ando, teiichi. *Anal. Chem.* 1985, **57**, 834-841.

76. Tiselius, A. *Trans. Faraday Soc.* 1937, **33**, 524.

77. Tsuda, T; Mizuno, T; Akiyama, J. *Anal. Chem.* 1987, **59**, 799.

78. Udseth, H. R.; Loo, J. A.; Smith, R. D. *Anal. Chem.* 1989, **61** (3), 228.

79. Vervoordeldonk, M. H. M. *Graduation report*, Eindhoven University of Technology, Eindhoven, 1977.

80. Virtanen, R. *Acta Polytech. Scand*, 1974, **123**, 1.

81. Wallingford, R.; Ewing, A. G. *Anal. Chem.* 1988, **60**, 1972.

82. Wallingford, R. A.; Ewing, A. G. *Anal. Chem.* 1987, **59**, 678 (1987).

83. Wallingford, R. and Ewing, A. G. *Anal. Chem.* 1987, **59**, 1762.

84. Wallingford, R. and Ewing, A. G. *Anal. Chem.* 1988, **60**, 258.

85. Wallingford, R.; Curry, P. D. Jr.; Ewing, A. G. *J. Microcolumn Sep.* 1989, **1** (1), 23.

86. Wallingford, R.; Ewing, A. G. *Anal. Chem.* 1989, **61**, 98.

87. Wallingford, R. and Ewing, A. G., Advances in Chromatography, 1989, **29**, 1-76.

88. *CRC Handbook of Chemistry and Physics*, 70 th Edition, R. C. Weast, CRC Press. Boca Raton, Florida (1989-1990).

76

89. Weston, Andrea; Brown, Phyllis R.; Heckenberg, Allan L.; Jandik, Peter; Jones, William R. *J. Chromatogr.* 1992, **602**, 249-256.

90. Wright, B. W.; Ross, G. A.; Smith, R. D. *J. Microcolumn. Sep.* 1989, **1**, 85.

91. Wu, S; Dovichi, N. J. *J. Chromatography*, 1989, **480**, 141.

92. Yeung, E. S.; Kuhr, W. G.; *Anal. Chem.* 1991, **63**, 275A.

93. Zhang, J. Z.; Chen, D. Y.; Wu, S. L.; Harke, H. R.; Dovichi, N. J., *Clinical Chemistry*, 1991, **37**, 1492.

94. *Chemical and Engineering News*, 1991, March 18, 58.

95. Model 1100 wafer dicing saw, operational mannual, Micro Automation Inc.

96. Stewart, J., *Calculas*, 2 nd edition, Brooks / Cole Publishing Company, Pacific Grove, California.

Appendix 1   **Estimation of the Limit of Detection (from reference 44)**
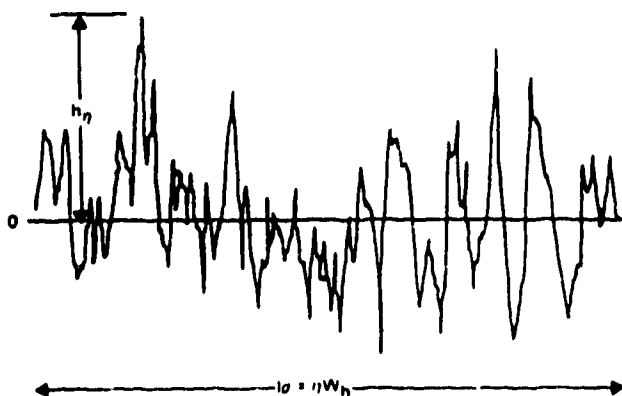
Detection limit is defined as the analyte concentration that produces a peak having a height equal to three times the standard deviation of the baseline noise. The largest noise fluctuation is measured in a chart interval that is a multiple of the analyte's peak width at one-half peak height. Knoll expressed the limit of detection (LOD):

$$C_{LOD} = K_{LOD}\, h_n\, C_s / h_s$$

where C_{LOD} is the concentration limit of detection, h_s / C_s is the peak height / unit amount of analyte. h_n is the largest noise fluctuation measured in the pre-selected chart interval. An example of a typical measurement is shown in the above figure. The K_{LOD} is a constant, determined for the measurement interval employed. The values of K_{LOD} are tabulated below:

Peak width multiple	K_{LOD}
10	1.9718
20	1.4309
50	0.9194
100	0.6536

Program for radially cutting through capillary

Program ID:	25
Mode:	10
Dimension 1:	60.000 mm
Dimension 2:	60.000 mm
1st index:	5.000 mm
2st index:	5.000 mm
Height:	0.076 mm
Thickness:	1.000 mm
Angle:	90.00
Cutting speed:	0.635 mm / sec.
Cutting increment:	0.508 mm
·pindle:	20000.0 RPM
Stop count:	999
Cut count:	1861

FIGURE 2.4 DICING PROGRAM

Program ID:	25
Mode:	10
Dimension 1:	30.000 mm
Dimension 2:	30.000 mm
1st index:	0.200 mm
2st index:	0.200 mm
Height:	0.160 mm (= 0.076 + 0.184 - 0.100)
Thickness:	1.000 mm
Angle:	90.00
Cutting speed:	0.635 mm / sec.
Cutting increment:	0.508 mm
Spindle:	20000.0 RPM
Stop count:	999
Cut count:	1861

FIGURE 2.5 DICING PROGRAM

Program ID:	25
Mode:	10
Dimension 1:	10.000 mm
Dimension 2:	10.000 mm
1st index:	5.000 mm
2st index:	5.000 mm
Height:	0.185 mm (= 0.076 + 0.184 - 0.075)
Thickness:	1.000 mm
Angle:	90.00
Cutting speed:	0.635 mm / sec.
Cutting increment:	0.508 mm
Spindle:	20000.0 RPM
Stop count:	999
Cut count:	1861

FIGURE 2.6 DICING PROGRAM

Program ID:	25
Mode:	10
Dimension 1:	20.000 mm
Dimension 2:	20.000 mm
1st index:	10.000 mm
2st index:	10.000 mm
Height:	0.277 mm (= 0.076 + 0.360 - 0.159)
Thickness:	1.000 mm
Angle:	90.00
Cutting speed:	0.635 mm / sec.
Cutting increment:	0.508 mm
Spindle:	20000.0 RPM
Stop count:	999
Cut count:	1861

FIGURE 2.7 DICING PROGRAM

Program ID:	22
Mode:	10
Dimension 1:	10.000 mm
Dimension 2:	10.000 mm
1st index:	0.150 mm
2st index:	0.150 mm
Height:	0.284 mm (= 0.076 + 0.363 - 0.155)
Thickness:	1.000 mm
Angle:	90.00
Cutting speed:	0.635 mm / sec.
Cutting increment:	0.508 mm
Spindle:	20000.0 RPM
Stop count:	999
Cut count:	1861

FIGURE 2.8 DICING PROGRAM

Program ID:	22
Mode:	10
Dimension 1:	10.000 mm
Dimension 2:	10.000 mm
1st index:	0.150 mm
2st index:	0.150 mm
Height:	20.141 mm (= 0.076 + 20.100 - 0.035)
Thickness:	22.000 mm
Angle:	90.00
Cutting speed:	0.635 mm / sec.
Cutting increment:	0.508 mm
Spindle:	20000.0 RPM
Stop count:	999
Cut count:	1861

FIGURE 2.9 DICING PROGRAM

Program ID:	22
Mode:	10
Dimension 1:	10.000 mm
Dimension 2:	10.000 mm
1st index:	0.150 mm
2st index:	0.150 mm
Height:	20.141 (0.076 + 20.1 - 0.035)
	20.151 mm (0.076 + 20.100 - 0.025)
	20.071 mm (0.076 + 20.100 - 0.105)
Thickness:	22.000 mm
Angle:	90.00
Cutting speed:	0.635 mm / sec.
Cutting increment:	0.508 mm
Spindle:	20000.0 RPM
Stop count:	999
Cut count:	1861

FIGURE 2.10 DICING PROGRAM

Program ID:	22
Mode:	10
Dimension 1:	10.000 mm
Dimension 2:	10.000 mm
1st index:	0.150 mm
2st index:	0.150 mm
Height:	20.071 mm (= 0.076 + 20.100 - 0.105)
	20.041 mm (= 0.076 + 20.100 - 0.135)
Thickness:	22.000 mm
Angle:	90.00
Cutting speed:	0.635 mm / sec.
Cutting increment:	0.508 mm
Spindle:	20000.0 RPM
Stop count:	999
Cut count:	1861

Appendix 3   Blue vinyl film (adhesive P / N 18074)

Blue vinyl film Adhesive P / N 18074 is a flexible polyvinyl chloride with a "medium" adhesion synthetic acrylic adhesive bonded to one side of the film. It is tough, has high tear strength and elongation. This plastic is used extentsively for Wafer sawing, Wafer scribing, Wafer expanding and die bonding.

Specifications

Color: light blue

Thickness: 76 μm

Elongation: 200 %

Adhesive: synthetic acrylic

Adhesion: 7 oz. / inch (medium tack) part # 18074

Core size: 3 inches I.D.

Form: Rolls 660 feet long and sheets on non-contaminating backing paper.

Semiconductor Equipment Corp.

5157 Goldman Avenue

Moorpark, CA 93020-0779

U.S.A.

Telephone: 805-529-2293, Fax: 805-529-2193.